Article

Cell

# Opposing Effects of Fasting Metabolism on Tissue Tolerance in Bacterial and Viral Inflammation

## Graphical Abstract

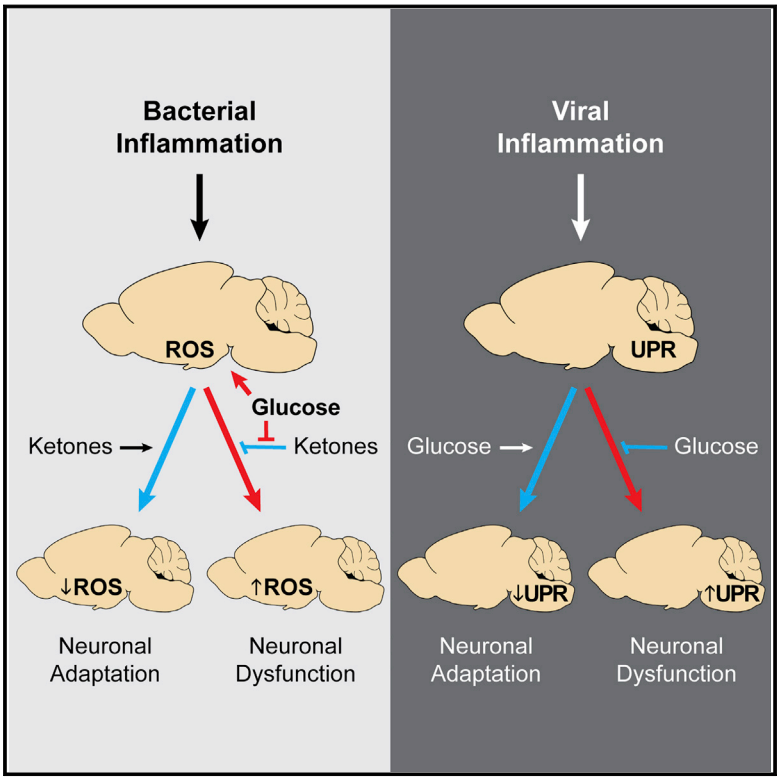


## Highlights

- Fasting metabolism is protective in bacterial, but not viral, inflammation
- Ketone bodies limit ROS-induced neuronal damage during bacterial inflammation
- Glucose utilization prevents UPR-mediated neuronal damage during viral inflammation

## Authors

Andrew Wang, Sarah C. Huen, Harding H. Luan, ..., Jean-Dominique Gallezot, Carmen J. Booth, Ruslan Medzhitov

## Correspondence

ruslan.medzhitov@yale.edu

## In Brief

Starve a fever, stuff a cold: why anorexia helps the organism to tolerate bacterial infections but makes viral infections hard to endure.

Wang et al., 2016, Cell *166*, 1512–1525
September 8, 2016 
http://dx.doi.org/10.1016/j.cell.2016.07.026

CellPress

Cell

Article

# Opposing Effects of Fasting Metabolism on Tissue Tolerance in Bacterial and Viral Inflammation

Andrew Wang,[1,2,7] Sarah C. Huen,[1,3,7] Harding H. Luan,[1,7] Shuang Yu,[1] Cuiling Zhang,[1] Jean-Dominique Gallezot,[4] Carmen J. Booth,[5] and Ruslan Medzhitov[1,6,8,*]

[1]Department of Immunobiology
[2]Department of Medicine (Rheumatology)
[3]Department of Medicine (Nephrology)
[4]Yale PET Center, Department of Radiology and Biomedical Imaging
[5]Section of Comparative Medicine
Yale University School of Medicine, New Haven, CT 06520, USA
[6]Howard Hughes Medical Institute, Chevy Chase, MD 20815, USA
[7]Co-first author
[8]Lead Contact
*Correspondence: ruslan.medzhitov@yale.edu
http://dx.doi.org/10.1016/j.cell.2016.07.026

## SUMMARY

**Acute infections are associated with a set of stereotypic behavioral responses, including anorexia, lethargy, and social withdrawal. Although these so-called sickness behaviors are the most common and familiar symptoms of infections, their roles in host defense are largely unknown. Here, we investigated the role of anorexia in models of bacterial and viral infections. We found that anorexia was protective while nutritional supplementation was detrimental in bacterial sepsis. Furthermore, glucose was necessary and sufficient for these effects. In contrast, nutritional supplementation protected against mortality from influenza infection and viral sepsis, whereas blocking glucose utilization was lethal. In both bacterial and viral models, these effects were largely independent of pathogen load and magnitude of inflammation. Instead, we identify opposing metabolic requirements tied to cellular stress adaptations critical for tolerance of differential inflammatory states.**

## INTRODUCTION

Sickness behaviors are a collection of prominent symptoms of acute illness that include anorexia, lethargy, fever, altered sleep patterns, depression, lack of grooming, and social withdrawal. It has been long appreciated that sickness behaviors are motivational states rather than a result of debilitation of physiological functions (Miller, 1964). Furthermore, sickness behaviors have been conceptualized as adaptive programs that promote survival of acute infections (Hart, 1988; Kluger et al., 1975). However, the mechanisms whereby different sickness behaviors contribute to survival remain largely unknown. This issue is particularly important because a popular treatment for acute infections is the use of non-steroidal anti-inflammatory drugs, which work primarily by suppressing the symptoms of sickness behaviors (Pecchi et al., 2009). Understanding the biology of sickness behaviors is also important for improved management of critically ill patients suffering from conditions with poorly defined pathogenesis, such as sepsis. Indeed, sepsis remains a largely intractable clinical problem with high mortality rates even in modern medical facilities (Angus and van der Poll, 2013). It is now increasingly appreciated that the mortality of sepsis can stem from at least three distinct phases of the disease: hemodynamic shock; multiple organ failure; and prolonged immunosuppression (Hotchkiss et al., 2013). Furthermore, different forms of sepsis can result from bacterial, fungal, and viral infections, each creating a distinct challenge and potentially requiring different management strategies.

Anorexia of infection is an aspect of sickness behavior that is conserved from humans to insects (Adamo, 2005), and much effort has been dedicated to understanding the role of nutrition in septic critical illness (Casaer and Van den Berghe, 2014). In the 1970s, it was demonstrated that interfering with the anorexia induced by *Listeria* infection using caloric supplementation led to pronounced mortality in mice (Murray and Murray, 1979; Wing and Young, 1980). Importantly, Ayres and Schneider (2009) found that, in *Drosophila*, anorexia was beneficial in some, but not all, infections. Similarly, it was recently shown that the fasting metabolic state was critical to surviving bacterial sepsis (Feingold et al., 2012). The mechanism remains elusive, and clinically, the role of nutrition in managing patients with sepsis is unclear.

An important new paradigm that can help explain at least some benefits of sickness behavior is the notion of resistance and tolerance: survival of infections can be promoted by either reducing pathogen burden or by increasing host tolerance to the damage of infection (Ayres and Schneider, 2012; Soares et al., 2014). During an infection, multiple physiological processes undergo dramatic alterations with often unknown rationale. Depending on the infection, these can include profound changes in metabolism and alterations in hepatic, renal, and cardiovascular functions. In principle, these responses can be either beneficial, induced as part of a general defense program,

or they can be unintended and detrimental but unavoidable consequences of infections. Furthermore, the physiological changes that are beneficial for host survival can contribute to elimination of pathogens (resistance) or to mitigation of tissue damage caused by infection (tolerance). These physiological responses are poorly understood aspects of infection biology, where most of the focus has been devoted to the immune response and microbial pathogenesis.

There are several examples where organismal metabolism has been shown to be regulated in order to deprive necessary substrates for pathogen viability as a strategy of enhancing host resistance (Liu et al., 2012; Nairz et al., 2015), but how organismal metabolic states, such as the fasted state of anorexia, contribute to host defense is not understood. Indeed, the role of metabolic homeostasis during sepsis, which is directly impacted by nutritional status, is becoming increasingly recognized as critical in surviving sepsis in the clinical setting. In addition to the well-studied but contentious role of glucose homeostasis in managing sepsis in the intensive care units (NICE-SUGAR Study Investigators et al., 2009; van den Berghe et al., 2001), the largest proteomic and metabolomic screen of patients with sepsis to date identified fatty acid, glucose, and beta-oxidation pathways as being discriminatory between survivors and non-survivors (Langley et al., 2013). Bacterial sepsis leads to a pro-lipolytic state, which affects the ability of target tissues to utilize glucose via glycolysis and alternative fuel sources, such as ketone bodies (KBs) and free fatty acids (FFAs) via oxidative phosphorylation (Agwunobi et al., 2000). Growing evidence suggests that a shift from glucose to KB/FFA utilization is protective in bacterial sepsis, and these studies largely rely on pharmacologic targeting of peroxisome proliferator-activated receptor alpha (PPAR$\alpha$), the master regulator of the ketogenic program and fasting metabolism (Budd et al., 2007; Cámara-Lemarroy et al., 2015). The role of substrate utilization in viral infections is even less understood (Greseth and Traktman, 2014). These metabolic changes are presumed to be protective, but their mechanism of protection remains obscure.

Here, we report that, whereas nutritional supplementation increased mortality of *Listeria monocytogenes* infection, it protected against lethality of influenza virus infection. The causative component of food was determined to be glucose, and this effect was largely independent of inflammation or pathogen burden. To study the differential effects of glucose metabolism in bacterial and viral inflammation and sepsis generally, we utilized lipopolysaccharide (LPS) and poly(I:C) models of sepsis and found that, whereas therapeutic blockade of glucose utilization with 2-deoxy-D-glucose (2DG) protected against LPS-mediated sepsis, it was uniformly lethal with poly(I:C) sepsis. We found that, whereas glucose was necessary for adaptation to and survival from the stress of antiviral inflammation by preventing initiation of endoplasmic reticulum (ER) stress-mediated apoptotic pathways, glucose prevented adaptation to the stress of bacterial inflammation by inhibiting ketogenesis, which was necessary for limiting reactive oxygen species (ROS) induced by anti-bacterial inflammation. Our study elucidates how specific metabolic programs are coupled to different types of inflammation to regulate tolerance to inflammatory damage.

## RESULTS

### Anorexia Protects against *L. monocytogenes* Infection

To assess the role of anorexia in infection, we revisited the model of listeriosis used in prior studies (Murray and Murray, 1979; Wing and Young, 1980). We confirmed that, upon infection with *L. monocytogenes*, mice exhibited a dose-dependent decrease in their food intake (Figure 1A) and that enteral supplementation by gavage of 1 kilocalorie twice daily (*bis in die* [BID]) starting 8 hr post-infection uniformly killed *L. monocytogenes*-infected mice (Figure 1B). The caloric content supplemented was one-fifth of healthy mouse daily food intake. Additionally, we found that gavage with an isocaloric isovolumetric amount of glucose alone was sufficient to cause 100% mortality in infected mice (Figure 1B). To exclude contributions from enteroendocrine incretin signaling, we injected glucose intraperitoneally (i.p.) at a dose iso-osmolar to PBS, which provided about 2% of normal daily caloric intake, and found that this was sufficient to recapitulate the lethal effects of enteral glucose (Figure 1C). To assess whether glucose was necessary for lethality, we injected *L. monocytogenes*-infected mice with 2DG and found that 2DG fully rescued mice from listeriosis-induced mortality (Figure 1C), consistent with previous work (Miller et al., 1998). Collectively, these data suggest that glucose is the component of food that is necessary and sufficient to mediate lethality in listeriosis when anorexia is blocked by force feeding.

We found that glucose treatment did not significantly affect bacterial burden or immune infiltration but did increase plasma interferon gamma (IFN$\gamma$) 24 hr post-infection (Figures 1D–1F and S1). In contrast, 2DG-treated mice had significantly decreased bacterial load compared to controls (Figure 1E). The decreased bacterial burden was not due to heightened immune response, as plasma IFN$\gamma$, plasma interleukin-6 (IL-6), and liver immune infiltrate were all decreased in 2DG-treated animals (Figures 1D–1F and S1). These data raised the possibility that 2DG was mediating clearance of *L. monocytogenes* through direct inhibition of bacterial growth. To address this, we tested the effect of 2DG on the growth of *L. monocytogenes* and on the antimicrobial activity of macrophages infected with *L. monocytogenes*. In both cases, 2DG administration did not affect bacterial growth (Figures 1G and 1H). Because the protective effect of anorexia during *L. monocytogenes* infection was neither mediated through conventional immune clearance mechanisms, nor was it due to inhibition of bacterial proliferation, we hypothesized that tissue-protective mechanisms may be at play.

### Inhibition of Glucose Utilization Is Protective in Endotoxemia

To examine the role of tissue tolerance in mediating the protective effects of anorexia in bacterial sepsis, we used the LPS sepsis model, where mortality results entirely from a systemic inflammatory response. We found that gavaging mice with enteral nutrition starting 1 hr post-LPS injection led to significantly increased mortality, whereas fluid resuscitation improved survival (Figure 2A). To dissect the nutritional components that contribute to mortality, we gavaged mice with isocaloric isovolumetric amounts of glucose, olive oil, or casein and found that

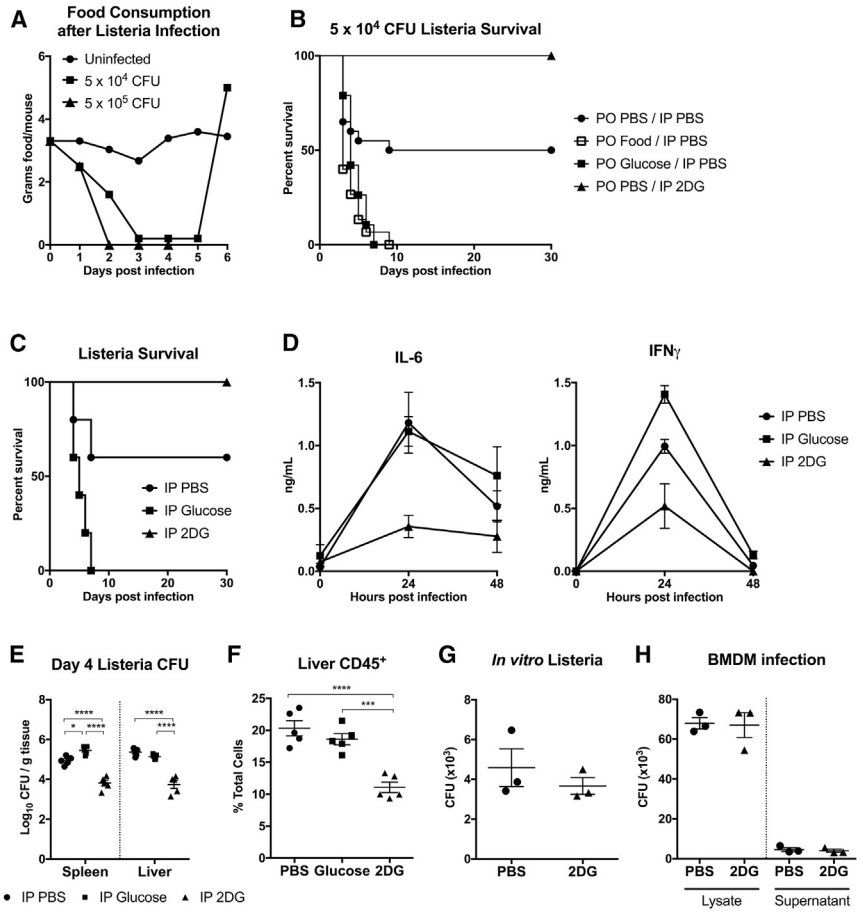


**Figure 1. Glucose Caloric Supplementation during *Listeria monocytogenes* Infection Worsens Survival, whereas 2DG Promotes Survival**

(A) Food consumption after infection with $5 \times 10^4$ and $5 \times 10^5$ colony-forming units (CFUs) wild-type *L. monocytogenes*.

(B) Survival after infection with $5 \times 10^4$ *L. monocytogenes*. Mice were per os (PO) gavaged with Abbott Promote (food), glucose, or PBS vehicle and injected intraperitoneally (IP) with 2DG or PBS. PO PBS/IP PBS n = 20; PO food/IP PBS n = 15 ($p = 0.0011$ versus PO PBS/IP PBS); PO glucose/IP PBS n = 19 ($p = 0.004$ versus PO PBS/IP PBS); PO PBS/IP 2DG n = 10 ($p = 0.0085$ versus PO PBS/IP PBS).

(C–F) Mice were infected with $5 \times 10^4$ CFUs *L. monocytogenes* and then treated with IP PBS, glucose, or 2DG. n = 5/group. (C) Survival after *L. monocytogenes* infection and indicated treatments is shown. PBS versus glucose $p = 0.0396$; PBS versus 2DG $p = 0.0344$; glucose versus 2DG $p = 0.0017$. (D) Plasma IL-6 and IFNγ 24 and 48 hr after $5 \times 10^4$ *L. monocytogenes* infection are shown. 24-hr plasma IL-6: PBS versus 2DG $p = 0.0005$; glucose versus 2DG $p = 0.0014$; 24-hr plasma IFNγ: PBS versus glucose; PBS versus 2DG; glucose versus 2DG all $p < 0.0001$. (E) *Listeria* CFUs from spleen and liver 4 days post-infection are shown. (F) Flow cytometry analysis of $CD45^+$ cells within the liver 4 days post-infection is shown. (G) CFU growth of *L. monocytogenes* after incubation in brain heart infusion broth with or without 15 mM 2DG for 18 hr.

(H) Bone-marrow-derived macrophages (BMDMs) were infected with $5 \times 10^5$ CFUs of *L. monocytogenes* in the presence or absence of 15 mM 2DG for 24 hr. CFUs of *L. monocytogenes* grown from the BMDM cell media supernatant and cell lysate.

Data are represented as mean ± SEM. $^*p < 0.05$; $^{***}p < 0.001$; $^{****}p < 0.0001$. See also Figure S1.

only glucose significantly increased mortality (Figure 2B). We then tested whether the effects of food intake on susceptibility to sepsis could be reversed with concurrent 2DG treatment. i.p. injection of 2DG concurrently with gavage of enteral nutrition in endotoxemic mice significantly improved survival (Figure 2C). As was the case in *L. monocytogenes* infection, i.p. injection of glucose was sufficient to uniformly kill endotoxemic mice whereas i.p. injection of 2DG was sufficient to fully rescue them (Figure 2D). To exclude contributions from carbohydrate-responsive element-binding protein (ChREBP) signaling, which would still be activated with 2DG, we utilized a glucose utilization inhibitor, D-mannoheptulose (DMH), which does not activate downstream ChREBP signaling (Li et al., 2010), and observed the same protective effects as 2DG (Figure S2A). Together, these data suggest that the component of nutritional intake that increased susceptibility to endotoxic shock was glucose and that inhibition of glucose utilization during sepsis was protective.

The advantage of the LPS sepsis model is that it isolates the inflammatory response, as opposed to direct pathogen toxicity, as the source of tissue damage. In this model, nutrients can affect survival by altering the magnitude of inflammatory response or the tissue's ability to tolerate it. We found no difference in circulating levels of tumor necrosis factor alpha (TNFα) and IL-6 or hepatic expression of acute phase-response genes in endotoxemic mice treated with PBS, glucose, or 2DG (Figures 2E and 2F). These findings suggest that glucose utilization does not affect the magnitude of the inflammatory response in endotoxic shock but rather the ability of the tissues to tolerate inflammatory damage.

## Glucose Utilization Promotes Tissue Damage in Endotoxemia

We observed that mice challenged with LPS and glucose displayed symptoms consistent with tonic-clonic seizure. Prior to death, animals would develop high-amplitude convulsions followed by decerebrate posturing. This is consistent with studies that have demonstrated neurologic deficits, including seizure, and neuronal apoptosis in animals suffering from endotoxic shock (Sayyah et al., 2003; Singer et al., 2016; Song et al., 2014). Hypoglycemia is a common cause of seizure, but we found that blood glucose did not differ significantly between groups over time (Figure S2B). We performed vital sign

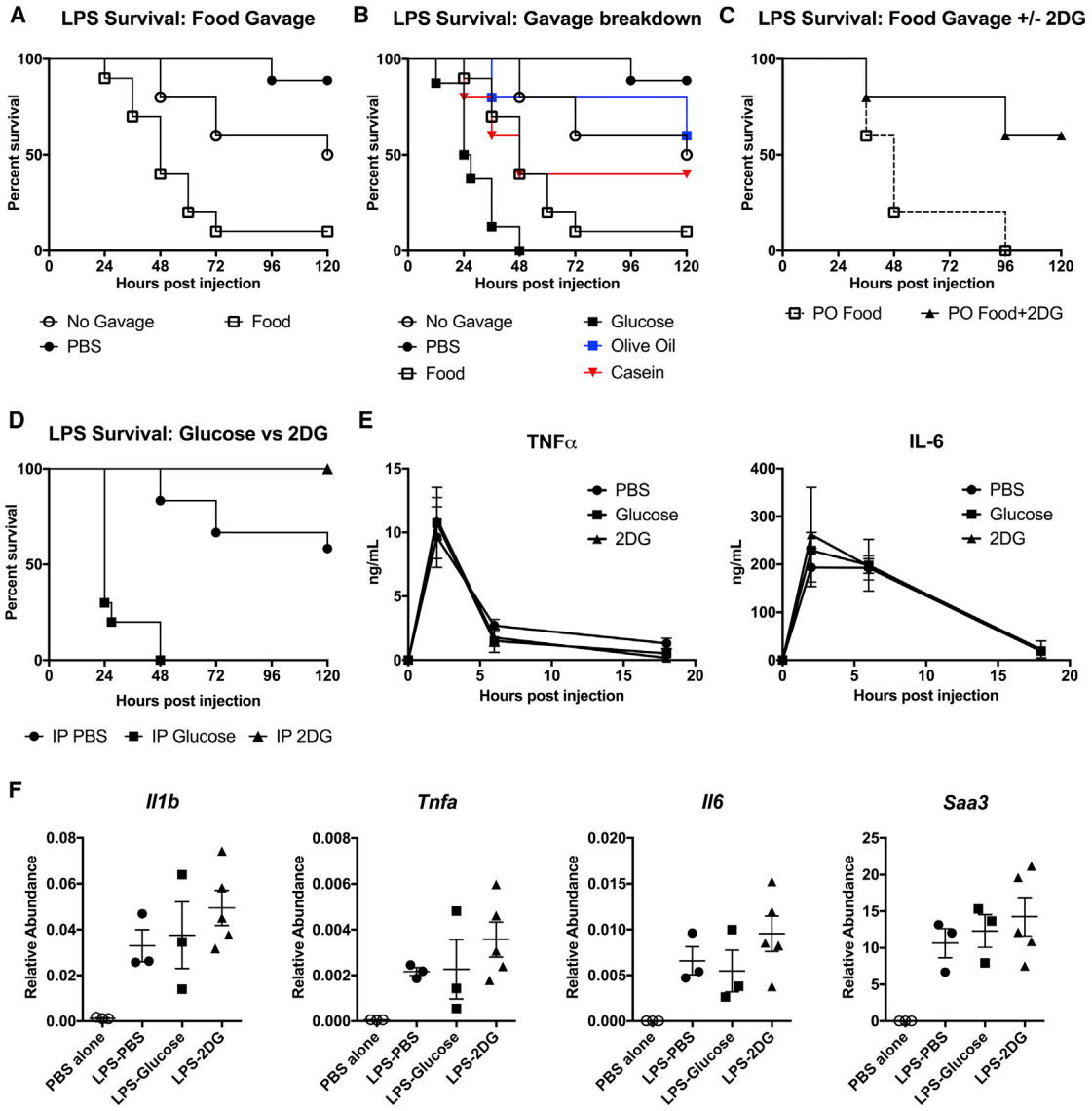


**Figure 2. Glucose Caloric Supplementation during LPS Sepsis Worsens Survival, whereas 2DG Promotes Survival**

(A and B) Survival after 15 mg/kg IP LPS and PO gavage with food, glucose, olive oil, casein, or PBS vehicle. PO PBS n = 10; PO food n = 10 ($p = 0.0002$ versus PO PBS); PO glucose n = 8 ($p < 0.0001$ versus PO PBS); no gavage n = 10 ($p = 0.0679$ versus PO PBS). (A) is a subset of (B), separated for clarity (the same PBS-treated, food-treated, and no gavage groups are shown in A and B).

(C) Survival after 15 mg/kg IP LPS and PO gavage with food with IP injections of PBS or 2DG. $p = 0.0433$.

(D–F) Mice were given 15 mg/kg IP LPS and then treated with IP PBS, glucose, or 2DG. (D) Survival after LPS and indicated treatments is shown. IP PBS n = 16; IP glucose n = 10 ($p < 0.0001$ versus IP PBS); IP 2DG n = 10 ($p = 0.01$ versus IP PBS). (E) Plasma TNFα and IL-6 are shown. n = 5–10/group. (F) Liver mRNA expression 4 hr after LPS and treatment with PBS (LPS-PBS), glucose (LPS-glucose), and 2DG (LPS-2DG) compared to PBS alone is shown. n = 3–5/group. Data are represented as mean ± SEM. See also Figure S2.

monitoring (body temperature, blood $O_2$ saturation, respiratory rate, and heart rate) in endotoxemic mice treated with PBS, glucose, or 2DG 24 hr post-LPS injection and found that 2DG-treated mice maintained their body temperature significantly better than glucose- and PBS-treated mice (Figure S2C). To assess other evidence of end-organ damage, we measured plasma markers of tissue injury (troponin-I, alanine aminotransferase, and creatinine), which were largely unchanged between treatments, with the exception that glucose-treated mice had higher levels of plasma creatinine (Figure S2D). Finally, detailed histopathologic analysis of H&E-stained slides of brain, heart, lung, liver, kidney, pancreas, stomach, bone marrow, thymus, and spleen was performed to identify any pathologic changes, including edema, hemorrhage, inflammation, necrosis, and apoptosis. The only difference in histopathologic changes was a decreased presence of dark, shrunken neurons in the brains

of LPS mice given 2DG, compared to mice given LPS and PBS or glucose. Together, these data implicate neuronal dysfunction as a possible proximal cause of death in LPS endotoxemia.

## Inhibition of Glucose Utilization Is Lethal in Influenza Infection

We next asked whether viral infections, which induce a different type of immune response compared to bacterial infections, were also affected by caloric supplementation. We employed an influenza model in which mice are infected intranasally with influenza virus A/WSN/33. We observed that mice infected with influenza also exhibited anorexia, albeit less severely than in *L. moncytogenes* infection (Figure 3A). Surprisingly, we found that gavage of 1 kilocalorie BID of enteral nutrition starting 8 hr post-infection protected mice from influenza-associated mortality (Figure 3B). Gavage of isocaloric isovolumetric glucose partially recapitulated the effect of enteral nutrition, whereas i.p. injection of 2DG concurrently with feeding completely ablated the survival benefit (Figure 3C). Caloric supplementation with casein and olive oil provided little to no survival benefit (Figure S3A). With a lower dose of influenza infection, we found that 2DG alone was able to uniformly kill flu-infected mice compared to vehicle control (Figure 3D). These data together indicate that glucose availability and utilization are critical to surviving influenza infection.

Next, we assessed whether the effect of caloric supplementation on influenza infection was mediated through immune resistance of virus or tissue tolerance. Differences in viral burden and/or immune activation would implicate an effect of caloric supplementation on host resistance. Six days post-infection, we performed plaque assays using both lung homogenate and bronchoalveolar lavage fluid (BAL) from mice treated with PBS or 2DG. Additionally, we assayed gene expression of the influenza gene *NP* from lung tissue homogenate. In all three cases, we found no differences in viral load between groups (Figure 3E). We then assayed antiviral inflammatory mediators to determine whether immunopathology could account for the lethality caused by 2DG treatment. We found that expression of interferon-inducible genes as well as *Cxcl1* and *Il6* were similar between PBS- and 2DG-treated groups (Figures 3F and S3B). Likewise, we found no difference in plasma IFNα levels or immune cell infiltration into the lung after infection (Figures 3G and S3C).

Mortality from influenza infection is often linked to development of pneumonia (Taubenberger and Morens, 2008). To determine whether 2DG impacted the extent of lung damage, we assessed the pathological outcomes of PBS versus 2DG treatment in influenza infection. Histopathologic examination of lung showed no difference in edema, hemorrhage, or inflammatory cell infiltrates (Figures 3H, 3I, and S3D). To identify alternative causes of death, we assayed vital signs of PBS- or 2DG-treated mice over the course of influenza infection. We found that 2DG-treated mice had no difference in blood $O_2$ level but had decreased heart rate, respiratory rate, and body temperature (Figure 3J). These findings are consistent with a derangement of central autonomic control. To verify that 2DG was not itself causing neuronal dysfunction and lethality, we administered the identical 2DG regimen utilized in influenza to mice infected with another pulmonary pathogen, *Legionella pneumophila*, and this did not cause mortality, indicating that the lethal effects of 2DG occurred only in the context of the viral inflammation induced by influenza infection (Figure S3E). Collectively, this suggests that the effect of caloric supplementation on influenza infection is mediated through availability of glucose utilization and its impact on tissue tolerance mechanisms, which are likely impaired in the brain.

## Inhibition of Glucose Utilization Is Lethal in Viral Inflammation

To generalize the findings from influenza infection, we next utilized intravenous poly(I:C) injection as a model of systemic viral inflammation (Smorodintsev et al., 1978). Co-administration of poly(I:C) and 2DG or DMH was uniformly lethal (Figures 4A and S4A). Because we were unable to generate a dose of poly(I:C) that caused lethality by itself, we were unable to assess whether glucose supplementation would be protective. To test whether type I IFN was required for the effect of 2DG on poly(I:C)-induced inflammation, we subjected IFNα-receptor (IFNaR)-deficient (*Ifnar1*$^{-/-}$) mice to poly(I:C) and 2DG challenge. *Ifnar1*$^{-/-}$ mice were completely protected (Figure 4B), indicating that IFNaR signaling was required for mediating the lethal effects of 2DG.

To examine whether the lethal effects of 2DG were mediated by differences in the magnitude of the inflammatory response, we assessed plasma cytokines and did not find significant differences in circulating IFNα (Figure 4C). Histopathologic analyses showed no differences between treatment groups. To identify the cause of mortality, we performed vital sign monitoring and found that mice challenged with poly(I:C) and 2DG, like flu-infected mice, exhibited profound defects in the control of body temperature and respiratory and heart rate, but not oxygen saturation (Figure 4D). Thus, we reasoned that neuronal dysfunction and loss of autonomic control was responsible for mortality.

## LPS- and Poly(I:C)-Induced Inflammation Cause Differential Glucose Uptake in the Brain

To globally assess 2DG and glucose uptake and distribution following poly(I:C) or LPS challenge, we subjected mice to 2-deoxy-2-[$^{18}$F] fluorodeoxy-D-glucose-positron emission tomography-computed tomography ($^{18}$F-FDG-PET-CT). We found that glucose was actively taken up by the brainstem after poly(I:C), but not with LPS challenge. In contrast, LPS induced more glucose uptake in the hypothalamic area (Figure 4E). There were no other differences in glucose compartmentalization between poly(I:C) and LPS (Figure S4B). Increased 2DG uptake in the hindbrain in poly(I:C)-treated mice was associated with decreased levels of *Il1b*, *Il6*, and *Tnfa* and no difference in *Mx1* in the hindbrain, indicating that neuronal dysfunction in brainstem was not due to increased inflammation (Figure S4C). Consistent with the PET data, we did not detect differences in blood glucose or measures of cardiac, liver, or renal dysfunction (Figure S4D).

These data suggest that the lethal effect of poly(I:C) and 2DG co-administration was likely independent of the magnitude of inflammation but rather was dependent on tissue tolerance

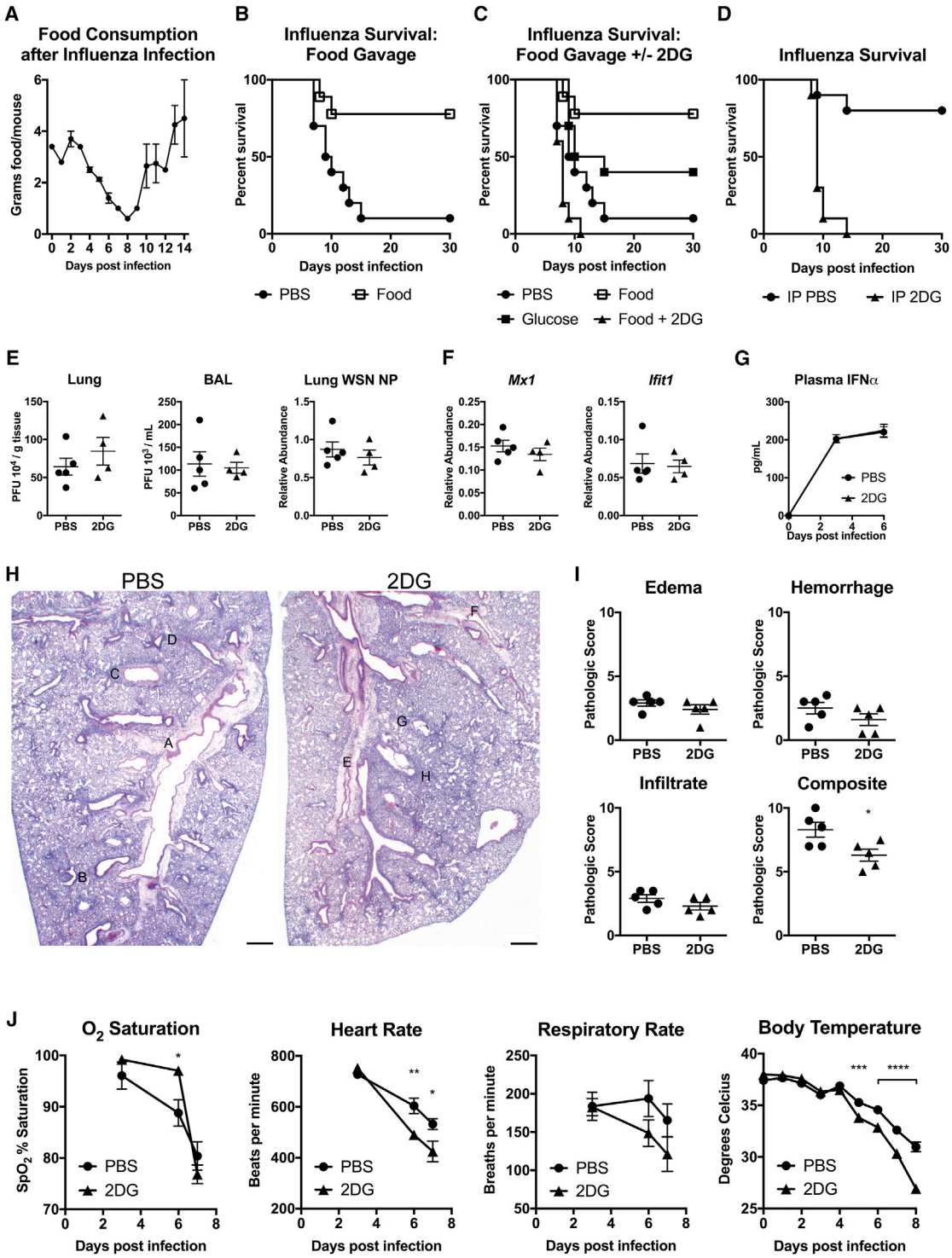


**Figure 3. Caloric Supplementation and Glucose Utilization Is Required for Surviving Influenza Infection**

(A) Food consumption after infection with 450 plaque forming units (PFUs) of influenza strain A/WSN/33.

(B and C) Survival after infection with 800 PFUs of influenza virus. Mice were gavaged with food, glucose, or PBS vehicle. Mice gavaged with food were also injected with IP PBS (food) or 2DG (food+2DG). PBS versus food $p = 0.0047$; PBS versus glucose $p = 0.1058$; food versus food+2DG $p = 0.0001$; PBS versus food+2DG $p = 0.0256$. n = 10/group. (B) is a subset of (C), separated for clarity (the same PBS-treated and food-treated groups are shown in B and C).

(D) Survival after infection with 375 PFUs of influenza virus and treatment with IP PBS or 2DG. $p < 0.0001$; n = 10/group.

*(legend continued on next page)*

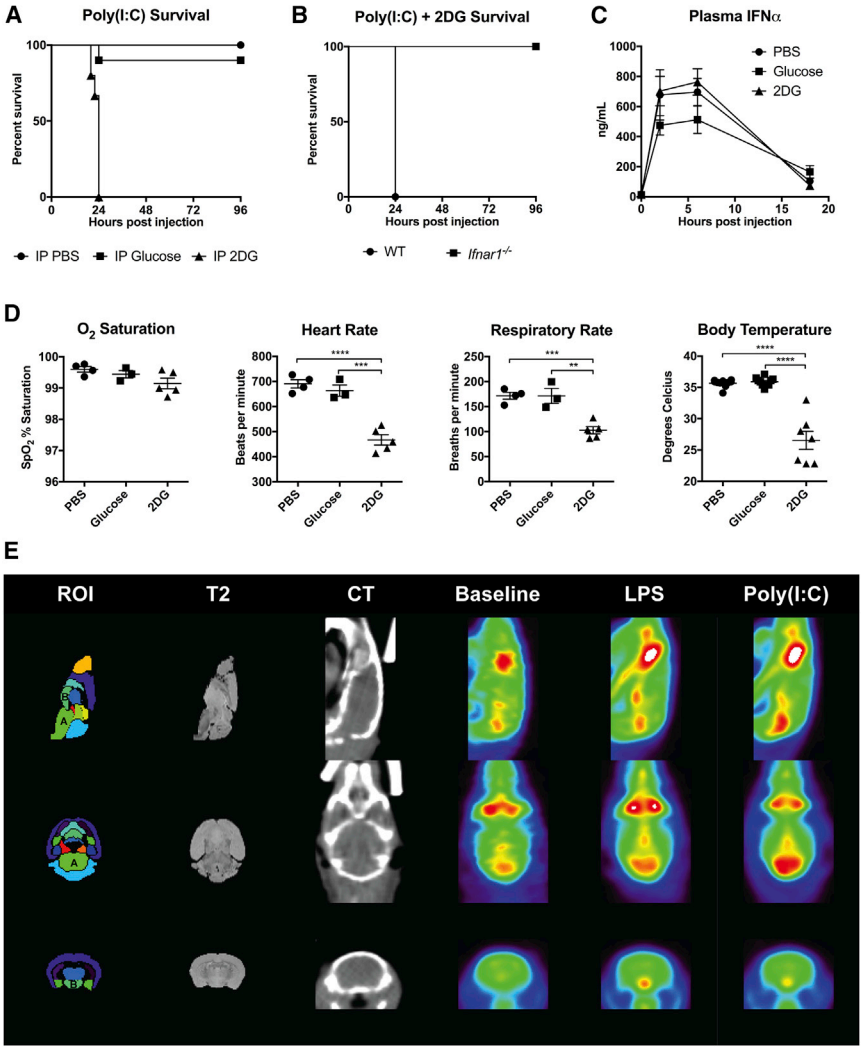


**Figure 4. Inhibition of Glucose Utilization Is Lethal in Poly(I:C) Inflammation**

(A) Survival of mice after poly(I:C) challenge and treatment with IP PBS, glucose, or 2DG. IP PBS n = 15, IP glucose n = 10 ($p = 0.2207$ versus IP PBS), and IP 2DG n = 15 ($p < 0.0001$ versus IP PBS).

(B) Survival of B6 wild-type (WT) mice and *Ifnar*$^{-/-}$ mice after poly(I:C) challenge and treatment with IP 2DG. WT versus *Ifnar*$^{-/-}$ $p = 0.0027$; n = 5/group.

(C and D) Mice were challenged with poly(I:C) and then treated with IP PBS, glucose, or 2DG. (C) Plasma IFNα is shown. n = 5/group. (D) Vital signs measured 18 hr after poly(I:C) administration are shown. n = 3–7/group.

(E) Averaged brain PET images after PBS vehicle (baseline), LPS, and poly(I:C) administration. "A" is the brainstem, and "B" is the hypothalamus. Anatomic atlas of regions of interest (ROIs) and T2-weighted magnetic resonance images are provided for reference. CT, computed tomography. n = 3/group.

Data are represented as mean ± SEM. $^{**}p < 0.01$; $^{***}p < 0.001$; $^{****}p < 0.0001$. See also Figure S4.

to immunopathology in the hindbrain, downstream of IFNaR signaling.

## Lethal Effect of 2DG in Viral Inflammation Is Mediated by CHOP

Because we found that mice displayed signs of neuronal damage in both influenza infection and poly(I:C)-induced viral inflammation, we further investigated the effect of inhibition of glucose utilization in viral inflammation. We reasoned that ER-stress-mediated apoptotic pathways, which are integral to the cellular response to viral infection, might link viral inflammation to neuronal damage (Lin et al., 2008). In particular, we focused on the ER-stress-induced transcription factor CHOP, which can induce apoptosis upon prolonged or excessive activation (Tabas and Ron, 2011). We found that expression of CHOP protein and its target gene *Gadd34* was elevated in the hindbrains of mice treated with poly(I:C) and 2DG, an effect that was IFNaR dependent (Figures 5A and 5B). Moreover, CHOP-deficient mice (*Ddit3*$^{-/-}$) were completely protected from poly(I:C) and 2DG challenge in a manner independent of inflammatory magnitude (Figures 5C and 5D). Autonomic dysfunction was also completely abrogated in CHOP-deficient mice challenged with poly(I:C) and 2DG (Figure 5E). To test the contribution of CHOP to host tolerance and resistance, we utilized the influenza infection model. We found that CHOP-deficient mice were significantly protected from influenza and 2DG challenge in a manner independent of pathogen burden or degree of inflammation (Figures 5F–5H and S5A). This is in contrast to models of bacterial inflammation, where CHOP deficiency promotes tissue injury and morbidity (Esposito et al., 2013). Interestingly, 2DG and IFNα together led to sustained and elevated CHOP expression and apoptosis in mouse embryonic fibroblasts (MEFs) (Figures S5B and S5C). These data together suggest that glucose utilization is critical to tissue tolerance of virally induced inflammation through maintenance of an appropriate ER stress response.

(E–J) Mice were infected with 375 PFUs influenza virus and treated with IP PBS or 2DG. n = 4–5/group. (E) Lung and bronchoalveolar lavage (BAL) viral load 6 days post-infection by PFU and qPCR for WSN nucleoprotein (NP) is shown. (F) mRNA expression of whole lung tissue at day 6 is shown. (G) Plasma IFNα is shown. (H and I) H&E staining of lung tissue 6 days post-infection and histologic scoring is shown. The scale bar represents 500 μm. For magnified views of insets, please see Figure S3E. (J) Vital signs after influenza infection are shown.

Data are represented as mean ± SEM. $^{*}p < 0.05$; $^{**}p < 0.01$; $^{***}p < 0.001$; $^{****}p < 0.0001$. See also Figure S3.

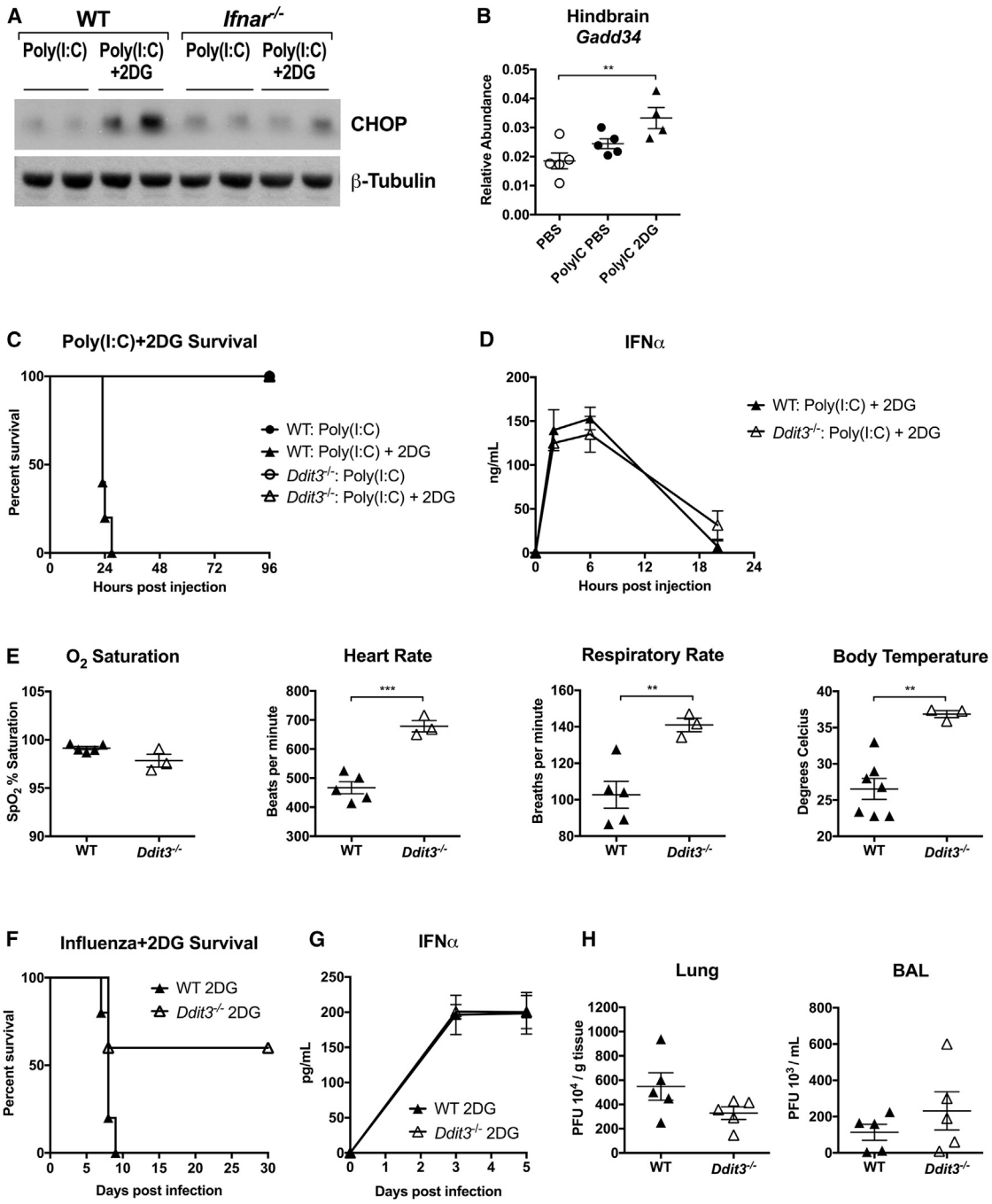


**Figure 5. Inhibition of Glucose Utilization in Poly(I:C)-Induced Inflammation Enhances ER Stress**

(A) WT and *Ifnar*$^{-/-}$ mice were challenged with poly(I:C) and then treated with either IP PBS or 2DG. Whole-hindbrain lysates 24 hr after poly(I:C) treatment immunoblotted for CHOP and β-tubulin are shown.

(B) Hindbrain mRNA expression of *Gadd34* 18 hr after poly(I:C) challenge and treatment with IP PBS or 2DG in WT mice. n = 5/group (one death in poly(I:C) group).

(C) Survival of WT mice and *Ddit3*$^{-/-}$ mice after poly(I:C) challenge and treatment with IP PBS or 2DG. WT: poly(I:C) + 2DG versus *Ddit3*$^{-/-}$: poly(I:C) + 2DG p = 0.0015. n = 5/group.

(D and E) WT and *Ddit3*$^{-/-}$ mice were challenged with poly(I:C) and treated with 2DG. (D) Plasma IFNα is shown. n = 5/group. (E) Vital signs measured 18 hr after poly(I:C) + 2DG are shown. n = 3–7/group (vital sign values of WT mice same as those in Figure 4D).

(F–H) WT mice and *Ddit3*$^{-/-}$ mice were infected with 700 PFUs of influenza virus and treated with 2DG. (F) Survival after influenza infection is shown. p = 0.048; n = 5/group. (G) Plasma IFNα is shown. n = 5/group. (H) Lung and BAL viral load 5 days post-infection is shown. n = 5/group.

Data are represented as mean ± SEM. **p < 0.01; ***p < 0.001. See also Figure S5.

### Glucose Promotes Neuronal ROS and Seizure-Induced Death in Bacterial Inflammation

Prolonged fasting results in hypoglycemia accompanied by lipolysis and followed by ketogenesis. In anorexia following acute LPS challenge, there was a decrease in blood glucose and an increase in plasma FFA, plasma beta-hydroxybutyrate (BHOB), and the fasting hormone FGF21 (Figures 6A and S2B). The switch to this fasting metabolic profile was ablated by glucose administration (Figure 6A). There was no appreciable difference in the kinetics of blood glucose subsequent to treatment with glucose or 2DG (Figure S2B).

We observed that the administration of glucose to LPS-challenged mice potentiated seizures, implicating neurotoxicity as a mechanism for death. We therefore asked whether anti-epileptic drugs would be sufficient to rescue glucose-mediated death and found that administration of valproic acid (VA), but not levetiracetam (two commonly used anti-epileptic agents), was able to completely rescue LPS-challenged mice treated with glucose (Figure 6B). The anti-epileptic effects of VA are incompletely understood but appear to impact HDAC-inhibition (HDACi), GABA transduction, and PI3K and calcium handling (Terbach and Williams, 2009). KBs have also been implicated as HDACi of the same class as VA and have recently been shown to coordinate gene expression programs that confer resistance to ROS-mediated damage (Shimazu et al., 2013). We thus hypothesized that the suppression of KBs by glucose administration may be inhibiting these HDACi-mediated ROS adaptation pathways. To test this, we utilized dihydroethidium staining to measure ROS in situ in the brains of LPS-challenged mice treated with glucose and observed increased ROS in the brains of these mice (Figure S6A). We also observed more TUNEL-positive nuclei in sections of mouse brain in glucose-treated mice compared to 2DG- or PBS-treated mice challenged with LPS (Figure S6B). All groups had TUNEL-positive nuclei in areas of lymphoid cell death (thymus and spleen), but there were no TUNEL-positive nuclei in any other tissues surveyed (heart, lung, liver, and kidney). The brain was the only tissue where differences in TUNEL-positive nuclei were seen between groups (Figures S6C and S6D); however, the amount of cell death, which was assessed in the hypothalamus—given PET localization—was not dramatically different, indicating that cellular dysfunction, and not necessarily cell death, was being potentiated by glucose administration. Together, these data suggest that the enhanced lethality caused by glucose supplementation in endotoxemia is likely mediated through increased ROS and neuronal dysfunction.

### Inhibition of the Ketogenic Program in Bacterial Inflammation, but Not Viral Inflammation, Results in Mortality

To test the role of ketogenesis in bacterial and viral inflammation, we subjected mice deficient in PPARα and FGF21 to LPS or influenza infection. Both PPARα- and FGF21-deficient mice displayed enhanced mortality after LPS administration (Figure 6C). We verified that PPARα-deficient mice have severely impaired ketogenesis following LPS challenge and did not observe significant changes in the level of BHOB in FGF21-deficient animals (Figure 6D), consistent with findings observed in the fasting state (Potthoff et al., 2009). We also did not detect an increase in systemic cytokines in PPARα-deficient mice (Figure 6E). We hypothesized that either the lack of FGF21 or the lack of alternative fuel sources, which were both suppressed after glucose supplementation, was the cause of mortality. Because FGF21 is a known downstream target of PPARα (Feingold et al., 2012; Inagaki et al., 2007), we tested whether defective FGF21 production was the causative lesion in PPARα deficiency. We reconstituted PPARα-deficient and FGF21-deficient mice with recombinant FGF21 and found that, whereas FGF21 was sufficient to rescue FGF21-deficient mice, it was not sufficient to rescue PPARα-deficient mice (Figure 6F), arguing that other aspects of the fasting program were necessary to mediate survival of LPS sepsis. Finally, VA, but not 2DG, was able to rescue PPARα mice challenged with LPS (Figure 6G), indicating that some aspect of VA action—likely its HDACi activity—was sufficient to rescue the lack of KBs in PPARα mice and also that the protective effects of 2DG required an intact ketogenic program.

Because ketotic pre-conditioning has been shown to improve other neurologic conditions, such as epilepsy (Levy et al., 2012), we tested whether it would improve survival in sepsis. We found that mice pre-fasted for 24 hr or mice fed ketogenic diets for 3 days displayed enhanced sensitivity to LPS despite generating adequate levels of KBs (Figures S7A and S7B). We excluded the possibility that ketoacidosis was driving death (Figure S7C). These data indicate that the activation of the ketogenic program must be temporally coupled to the course of the inflammatory challenge.

We hypothesized that, because our viral and bacterial models had opposite dependencies on glucose, they would also have opposite dependencies on ketogenesis. Therefore, we subjected PPARα-deficient mice to influenza challenge. Whereas PPARα deficiency was lethal following LPS challenge, it was protective in influenza infection in a manner independent of pathogen control (Figures 6H and 6I). This protective effect was not observed in FGF21-deficient animals (Figure S7D). Together, these data show that, whereas impairment of ketogenesis, whether through genetic deletion of PPARα or glucose administration, was lethal in bacterial inflammation, it was protective in viral inflammation, in a manner independent of the magnitude of inflammation.

## DISCUSSION

Here, we addressed the effect of anorexia during acute infection and uncovered a surprising differential role for fasting metabolism in maintaining tissue tolerance in different infectious states. It is increasingly appreciated that inflammatory responses must be coupled to specific metabolic programs to support their energetic demands (Buck et al., 2015; Galván-Peña and O'Neill, 2014). In this study, we observed that systemic metabolism appears to be coordinated to support tolerance to different inflammatory states. We found that, whereas glucose utilization was required for survival in models of viral inflammation, it was lethal in models of bacterial inflammation. Concordantly, we found that, whereas ketogenesis was required for survival in bacterial inflammation, it was dispensable in the case of

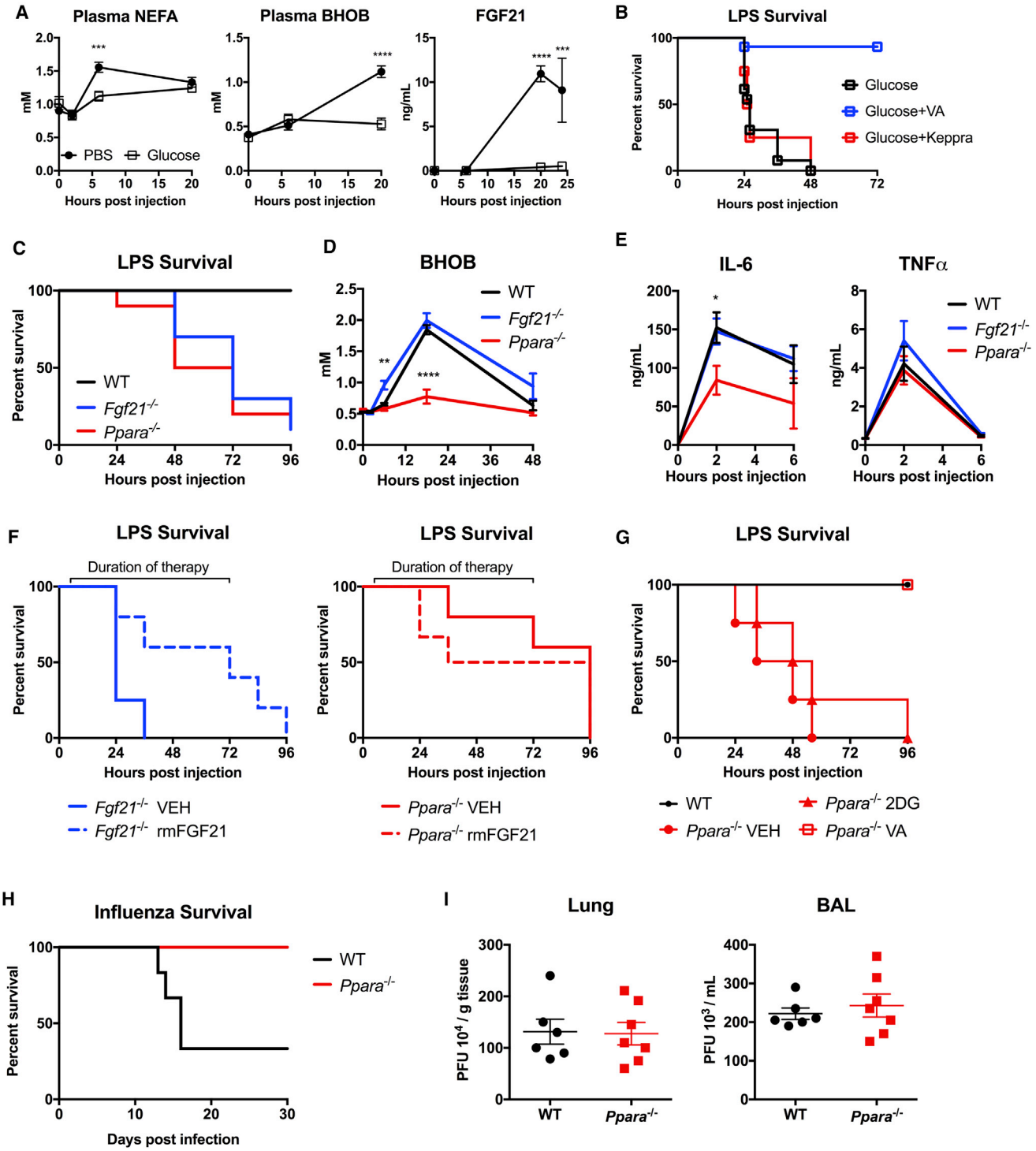


**Figure 6. Role of Ketogenic Program in Surviving Bacterial, but Not Viral, Inflammation**

(A) Plasma nonesterified fatty acids (NEFA), beta-hydroxybutyrate (BHOB), and fibroblast growth factor 21 (FGF21) after LPS, with treatment with IP PBS or glucose. n = 10/group.

(B) Survival after 8 mg/kg IP LPS and treatment with glucose. Mice were treated with vehicle, valproic acid (VA), or levetiracetam (Keppra) starting 6 hr after LPS. $p < 0.0001$ for glucose+VA versus glucose and glucose+VA versus glucose+Keppra. n = 15 glucose; n = 15 glucose+VA; n = 4 glucose+Keppra.

(C) Survival after 12.5 mg/kg IP LPS in WT, *Fgf21*$^{-/-}$, and *Ppara*$^{-/-}$ mice. n = 10/group. $p < 0.0001$ for WT versus *Fgf21*$^{-/-}$; $p = 0.0003$ for WT versus *Ppara*$^{-/-}$.

(D) Plasma BHOB after 12.5 mg/kg IP LPS in WT, *Fgf21*$^{-/-}$, and *Ppara*$^{-/-}$ mice. n = 4–6/group.

*(legend continued on next page)*

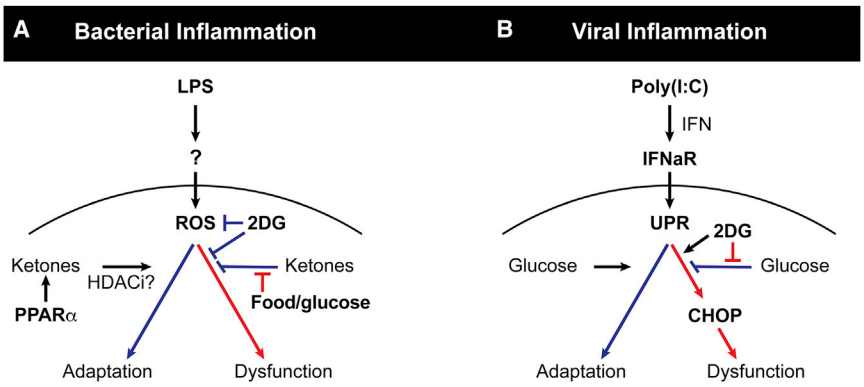


**Figure 7. Model of Glucose Utilization during Viral- and Bacterial-Mediated Inflammation Supporting Unique Tissue Tolerance Mechanisms**

(A) Glucose inhibits PPARα-dependent ketogenesis and cellular adaptation programs required for tissue tolerance during LPS and *Listeria*-mediated (bacterial) inflammation. Ketones act as fuel source and as HDACi, allowing for cellular and tissue adaptation. Inhibition of glucose utilization during bacterial inflammation with 2DG protects against tissue dysfunction and organismal mortality.

(B) Glucose utilization is required for adaptation to poly(I:C)- and influenza-mediated (viral) sepsis. Viral inflammation activates ER stress and the unfolded protein response (UPR) downstream of type I interferon signaling through IFNaR. Inhibition of glucose utilization in viral inflammation with 2DG enhances ER stress through a CHOP-dependent pathway, leading to tissue dysfunction and death.

viral inflammation. Unexpectedly, we found that these effects on mortality were largely independent of the degree of inflammation and pathogen clearance. In the case of viral inflammation, lethality subsequent to inhibition of glucose utilization appeared to be mediated by type I IFN signaling on target tissues—likely the brain—which require glucose to mitigate the ER stress response and CHOP-mediated cellular dysfunction. In the case of bacterial inflammation, lethality subsequent to glucose administration appeared to be mediated by suppression of ketogenesis, which led to impaired resistance to ROS-mediated damage in the brain (Figure 7). Thus, our results suggest that distinct inflammatory responses may be coupled with specific metabolic programs in order to support unique tissue tolerance mechanisms that, when uncoupled, lead to enhanced immunopathology, leading to death.

Host defense from infections involves both resistance and tolerance mechanisms. Whereas host resistance promotes pathogen clearance, host tolerance relies on adaptation to a given level of pathogen or a given level of inflammatory response (Råberg et al., 2007; Schneider and Ayres, 2008). Disease morbidity and mortality can be a result of either inadequate or impaired host resistance, characterized by high pathogen burden, or impaired host tolerance. Immunopathology falls into the latter category, and insufficient tissue protection is likely to be an important determinant in conditions characterized by excessive inflammation, such as sepsis. Tissue protection is likely a function of cellular stress adaptation pathways, which allow cells to survive noxious states, such as increased free radicals and accumulation of unfolded proteins (Figueiredo et al., 2013; Larsen et al., 2010). When these adaptation pathways are overwhelmed, cells can undergo apoptotic cell death (Boison, 2013; Tabas and Ron, 2011). Thus, one important determinant of host tolerance may be related to the ability of cellular adaptation programs to tolerate noxious states found in infections (Medzhitov et al., 2012). Because different infections generate different inflammatory responses and noxious states, specific cellular adaption programs would need to be activated in distinct infectious contexts.

We found that interfering with the normal ketogenic state following LPS-mediated inflammation was lethal, likely by interfering with ROS adaption programs in the brain. Our findings are consistent with observations that PPARα agonism and inhibition of glucose utilization are generally protective in bacterial sepsis models (Budd et al., 2007; Cámara-Lemarroy et al., 2015; Yoo et al., 2013). However, unlike many of these studies, we did not observe large differences in the magnitude of inflammation, likely because we administered 2DG and glucose after and not before infectious or inflammatory challenge. Thus, our observations are likely unrelated to the body of literature that supports a role for HIF1α, PKM2, and aerobic glycolysis in generating the LPS inflammatory response (Liu et al., 2016; Yang et al., 2014). Consistent with our inability to detect differences in inflammation in sterile inflammatory models, we did not detect differences in pathogen burden in live infection models where glucose administration led to lethality in *L. monocytogenes* infection in the absence of increased pathogen burden or bolstered immune response.

ROS-mediated cytotoxicity is a well-appreciated phenomenon in bacterial sepsis (Hoetzenecker et al., 2012; Kolls, 2006), and ROS-detoxification pathways have been implicated in

(E) Plasma IL-6 and TNFα in WT, *Fgf21*$^{-/-}$, and *Ppara*$^{-/-}$ mice after LPS. n = 5/group; *p < 0.05.

(F) Survival after 12.5 mg/kg IP LPS in *Fgf21*$^{-/-}$ and *Ppara*$^{-/-}$ mice, treated with i.v. 5 ng recombinant mouse FGF21 (rmFGF21) twice daily starting 6 hr after LPS injection. n = 5–6/group. p = 0.0491 *Fgf21*$^{-/-}$ VEH versus *Fgf21*$^{-/-}$ rmFGF21. p = 0.5767 *Ppara*$^{-/-}$ VEH versus *Ppara*$^{-/-}$ rmFGF21.

(G) Survival after 8 mg/kg IP LPS in WT and *Ppara*$^{-/-}$ mice. 2DG treatment was initiated 1 hr after LPS. VA was initiated 6 hr after LPS. n = 4–5/group. p = 0.0177 *Ppara*$^{-/-}$ VEH versus *Ppara*$^{-/-}$ VA.

(H and I) WT and *Ppara*$^{-/-}$ mice were infected with 400 PFUs of influenza virus. (H) Survival after influenza infection is shown. p = 0.0074; WT n = 6; *Ppara*$^{-/-}$ n = 8, representative of three independent experiments. (I) Lung and BAL viral load 5 days post-infection is shown. n = 6–7/group.

Data are represented as mean ± SEM. *p < 0.05; **p < 0.01; ***p < 0.001; ****p < 0.0001. See also Figures S6 and S7.

mitigating tissue damage and mortality. Shimazu et al. (2013) recently reported that BHOB functioned as an HDAC-1 inhibitor and that this led to transcription of ROS-detoxification pathways. Furthermore, we found that the timing of ketogenesis, an adequately nourished host, or both are necessary for the protective effect of fasting that occurs as a coordinated response to bacterial inflammation. Instead of rescuing mice from LPS mortality, fasting and ketogenic pre-conditioning potentiated death. Taken together, we present evidence that the fasting response that occurs as part of the inflammatory response is required to maintain resistance to oxidative stress in LPS sepsis.

Although anorexia is a common response in both bacterial and viral infections, we find the opposite consequence of fasting metabolism in our models of bacterial and viral inflammation. Whereas in bacterial infection and LPS-induced inflammation, we found a detrimental effect of glucose, a protective effect of 2DG, and a requirement for ketogenesis in order to maintain tolerance, in viral infection and poly(I:C)-induced inflammation, these effects were opposite. 2DG administration led to lethality in poly(I:C)-induced inflammation in a manner that was independent of the magnitude of IFN$\alpha$ expression but dependent on IFNaR signaling. Manipulation of fasting metabolism did not affect viral burden in influenza infection. Viral infections are known to stimulate the unfolded protein response mediated, in part, via the PERK-eIF2a-ATF4-CHOP pathway (Janssens et al., 2014). When this pathway is engaged, cells can either adapt to ER stress or induce apoptosis through CHOP if ER stress cannot be managed (Tabas and Ron, 2011). Our data suggest that glucose utilization is required for the cytoprotective response in neurons in the setting of viral inflammation, as inhibition of glucose utilization led to death, which was CHOP dependent. Indeed, our PET studies indicate that glucose redistribution is largely the same between the early phases of bacterial and viral inflammatory challenge with the exception of sub-regions in the brain, where LPS and poly(I:C) appear to regulate glucose uptake differentially. The purpose and mechanism underlying this observation remain to be elucidated. The precise mechanism whereby IFN signaling converges with glucose utilization programs also remains to be fully resolved, but recent studies demonstrated that interferon signaling leads to changes in glucose uptake, which is important for the antiviral response (Burke et al., 2014). Thus, whereas alternative fuel substrate availability is coupled to and necessary for adaptation to bacterial inflammation, glucose availability is coupled to and necessary for cellular adaptation to viral inflammation. The logic of their coupling is likely related to the substrate dependence of the cellular adaptation programs that are engaged. These findings are consistent with our previous study, where we found that synergistic lethality in mice co-infected with influenza and *Legionella* occurred in a manner independent of pathogen burden (Jamieson et al., 2013), and it is interesting to speculate here that perhaps one cause of lethality in this co-infection model is a result of metabolic incompatibility in the setting of both a viral and bacterial infection.

Given the conservation of cellular adaptation and metabolic programs in mouse and human, our findings likely have clinical implications. The role of nutrition in managing patients with sepsis is unclear at best, and multiple studies have failed to show differences in survival from feeding, including the most-recent study, which asked whether lower caloric supplementation would improve outcomes (Arabi et al., 2015). There have been a series of studies exploring different feeding formulations with different caloric or micronutrient contents (Casaer and Van den Berghe, 2014). However, we could not find an example where different feeding formulations were targeted to different types of infections, as opposed to different types of organ failure (Seron-Arbeloa et al., 2013), or where post hoc analyses were directed at pathogen class. Our study implicates a differential need for metabolic fuels as a function of infection (or inflammation) class and sheds light on the biology behind the old adage "starve a fever, stuff a cold." Much work will need to be done to identify how organismal metabolism is coordinated in other infectious and inflammatory states and whether or not these findings can be extended to humans in the management of inflammatory diseases and critical illness.

## Limitations, Caveats, and Open Questions

One limitation of this study (common to most animal studies) is that it was performed on a single mouse strain (C57BL/6J) in one mouse facility. Thus, the roles of genetic background and facility-specific environment remain unknown. In addition, there are many caveats with extrapolating data on organismal biology from studies in unnatural settings of animal facilities. There are also many open questions raised by this study, including why are different brain regions differentially affected by bacterial and viral inflammation? What are intrinsic properties of the affected neurons that make them susceptible to damage, depending on inflammatory pathway and available metabolic fuels? Finally, it remains to be seen how these results apply to critical illness in humans.

## STAR★METHODS

Detailed methods are provided in the online version of this paper and include the following:

- KEY RESOURCES TABLE
- CONTACT FOR REAGENT AND RESOURCE SHARING
- EXPERIMENTAL MODEL AND SUBJECT DETAILS
  - Mice
  - Cell Culture
- METHOD DETAILS
  - Quantification of Bacterial and Viral Loads
  - Plasma Cytokine, Metabolite, and Tissue Injury Marker Analysis
  - RNA Extraction and Quantification
  - Flow Cytometry
  - In Vivo Reactive Oxygen Species Staining
  - Positron-Emission Tomography and Analyses
  - Histopathlogy
  - Western Blot
- QUANTIFICATION AND STATISTICAL ANALYSIS

### SUPPLEMENTAL INFORMATION

Supplemental Information includes seven figures and one table and can be found with this article online at http://dx.doi.org/10.1016/j.cell.2016.07.026.

A video abstract is available at http://dx.doi.org/10.1016/j.cell.2016.07.026#mmc2.

## AUTHOR CONTRIBUTIONS

A.W., S.C.H., and H.H.L. contributed equally to this work. A.W., S.C.H., H.H.L., and R.M. designed the study, analyzed the data, and wrote the manuscript with input from the other authors. A.W., S.C.H., and H.H.L. performed the experiments with assistance from S.Y. and C.Z. J.-D.G. performed all analyses for PET studies. C.J.B. evaluated tissue histology.

## ACKNOWLEDGMENTS

We thank members of the R.M. lab for helpful discussions, Marya Shanabrough and Tamas Horvath for help with processing of brain specimens, and David Mangelsdorf and Steven Kliewer for making available the *Fgf21*$^{-/-}$ mice. This study was supported by the HHMI, Else Kröner Fresenius Foundation, The Blavatnik Family Foundation, and grants from the NIH (AI046688, AI089771, and CA157461). A.W. was supported by NIH grant T32 AR07107-39. S.C.H. was supported by American Heart Association grant 13FTF17070000. H.H.L. was supported by the Gruber Science Fellowship. Plasma creatinine was processed through the Yale George M. O'Brien Kidney Center, NIH grant P30-DK079310. Preparation of histology sections were performed by the Yale Research Pathology and Histology Core.

Received: April 15, 2016
Revised: June 21, 2016
Accepted: July 19, 2016
Published: September 8, 2016

## REFERENCES

Adamo, S.A. (2005). Parasitic suppression of feeding in the tobacco hornworm, Manduca sexta: parallels with feeding depression after an immune challenge. Arch. Insect Biochem. Physiol. *60*, 185–197.

Agwunobi, A.O., Reid, C., Maycock, P., Little, R.A., and Carlson, G.L. (2000). Insulin resistance and substrate utilization in human endotoxemia. J. Clin. Endocrinol. Metab. *85*, 3770–3778.

Angus, D.C., and van der Poll, T. (2013). Severe sepsis and septic shock. N. Engl. J. Med. *369*, 840–851.

Arabi, Y.M., Aldawood, A.S., Haddad, S.H., Al-Dorzi, H.M., Tamim, H.M., Jones, G., Mehta, S., McIntyre, L., Solaiman, O., Sakkijha, M.H., et al.; PermiT Trial Group (2015). Permissive underfeeding or standard enteral feeding in critically ill adults. N. Engl. J. Med. *372*, 2398–2408.

Archer, K.A., and Roy, C.R. (2006). MyD88-dependent responses involving toll-like receptor 2 are important for protection and clearance of Legionella pneumophila in a mouse model of Legionnaires' disease. Infect Immun. *74*, 3325–3333.

Auerbuch, V., Brockstedt, D.G., Meyer-Morse, N., O'Riordan, M., and Portnoy, D.A. (2004). Mice lacking the type I interferon receptor are resistant to Listeria monocytogenes. J. Exp. Med. *200*, 527–533.

Ayres, J.S., and Schneider, D.S. (2009). The role of anorexia in resistance and tolerance to infections in *Drosophila*. PLoS Biol. *7*, e1000150.

Ayres, J.S., and Schneider, D.S. (2012). Tolerance of infections. Annu. Rev. Immunol. *30*, 271–294.

Boison, D. (2013). Chopping out CHOP chops the fate of neurons. Epilepsy Curr. *13*, 219–220.

Buck, M.D., O'Sullivan, D., and Pearce, E.L. (2015). T cell metabolism drives immunity. J. Exp. Med. *212*, 1345–1360.

Budd, A., Alleva, L., Alsharifi, M., Koskinen, A., Smythe, V., Müllbacher, A., Wood, J., and Clark, I. (2007). Increased survival after gemfibrozil treatment of severe mouse influenza. Antimicrob. Agents Chemother. *51*, 2965–2968.

Burke, J.D., Platanias, L.C., and Fish, E.N. (2014). Beta interferon regulation of glucose metabolism is PI3K/Akt dependent and important for antiviral activity against coxsackievirus B3. J. Virol. *88*, 3485–3495.

Cámara-Lemarroy, C.R., Guzman-DE LA Garza, F.J., Cordero-Perez, P., Ibarra-Hernandez, J.M., Muñoz-Espinosa, L.E., and Fernandez-Garza, N.E. (2015). Gemfibrozil attenuates the inflammatory response and protects rats from abdominal sepsis. Exp. Ther. Med. *9*, 1018–1022.

Casaer, M.P., and Van den Berghe, G. (2014). Nutrition in the acute phase of critical illness. N. Engl. J. Med. *370*, 1227–1236.

Esposito, V., Grosjean, F., Tan, J., Huang, L., Zhu, L., Chen, J., Xiong, H., Striker, G.E., and Zheng, F. (2013). CHOP deficiency results in elevated lipopolysaccharide-induced inflammation and kidney injury. Am. J. Physiol. Renal Physiol. *304*, F440–F450.

Feingold, K.R., Grunfeld, C., Heuer, J.G., Gupta, A., Cramer, M., Zhang, T., Shigenaga, J.K., Patzek, S.M., Chan, Z.W., Moser, A., et al. (2012). FGF21 is increased by inflammatory stimuli and protects leptin-deficient ob/ob mice from the toxicity of sepsis. Endocrinology *153*, 2689–2700.

Figueiredo, N., Chora, A., Raquel, H., Pejanovic, N., Pereira, P., Hartleben, B., Neves-Costa, A., Moita, C., Pedroso, D., Pinto, A., et al. (2013). Anthracyclines induce DNA damage response-mediated protection against severe sepsis. Immunity *39*, 874–884.

Galván-Peña, S., and O'Neill, L.A. (2014). Metabolic reprograming in macrophage polarization. Front. Immunol. *5*, 420.

Greseth, M.D., and Traktman, P. (2014). De novo fatty acid biosynthesis contributes significantly to establishment of a bioenergetically favorable environment for vaccinia virus infection. PLoS Pathog. *10*, e1004021.

Hart, B.L. (1988). Biological basis of the behavior of sick animals. Neurosci. Biobehav. Rev. *12*, 123–137.

Hoetzenecker, W., Echtenacher, B., Guenova, E., Hoetzenecker, K., Woelbing, F., Brück, J., Teske, A., Valtcheva, N., Fuchs, K., Kneilling, M., et al. (2012). ROS-induced ATF3 causes susceptibility to secondary infections during sepsis-associated immunosuppression. Nat. Med. *18*, 128–134.

Hotchkiss, R.S., Monneret, G., and Payen, D. (2013). Sepsis-induced immunosuppression: from cellular dysfunctions to immunotherapy. Nat. Rev. Immunol. *13*, 862–874.

Inagaki, T., Dutchak, P., Zhao, G., Ding, X., Gautron, L., Parameswara, V., Li, Y., Goetz, R., Mohammadi, M., Esser, V., et al. (2007). Endocrine regulation of the fasting response by PPARalpha-mediated induction of fibroblast growth factor 21. Cell Metab. *5*, 415–425.

NICE-SUGAR Study Investigators, Finfer, S., Chittock, D.R., Su, S.Y., Blair, D., Foster, D., Dhingra, V., Bellomo, R., Cook, D., Dodek, P., et al. (2009). Intensive versus conventional glucose control in critically ill patients. N. Engl. J. Med. *360*, 1283–1297.

Jamieson, A.M., Pasman, L., Yu, S., Gamradt, P., Homer, R.J., Decker, T., and Medzhitov, R. (2013). Role of tissue protection in lethal respiratory viral-bacterial coinfection. Science *340*, 1230–1234.

Janssens, S., Pulendran, B., and Lambrecht, B.N. (2014). Emerging functions of the unfolded protein response in immunity. Nat. Immunol. *15*, 910–919.

Kluger, M.J., Ringler, D.H., and Anver, M.R. (1975). Fever and survival. Science *188*, 166–168.

Kolls, J.K. (2006). Oxidative stress in sepsis: a redox redux. J. Clin. Invest. *116*, 860–863.

Langley, R.J., Tsalik, E.L., van Velkinburgh, J.C., Glickman, S.W., Rice, B.J., Wang, C., Chen, B., Carin, L., Suarez, A., Mohney, R.P., et al. (2013). An integrated clinico-metabolomic model improves prediction of death in sepsis. Sci. Transl. Med. *5*, 195ra95.

Larsen, R., Gozzelino, R., Jeney, V., Tokaji, L., Bozza, F.A., Japiassú, A.M., Bonaparte, D., Cavalcante, M.M., Chora, A., Ferreira, A., et al. (2010). A central role for free heme in the pathogenesis of severe sepsis. Sci. Transl. Med. *2*, 51ra71.

Levy, R.G., Cooper, P.N., and Giri, P. (2012). Ketogenic diet and other dietary treatments for epilepsy. Cochrane Database Syst. Rev. (3), CD001903.

Li, M.V., Chen, W., Harmancey, R.N., Nuotio-Antar, A.M., Imamura, M., Saha, P., Taegtmeyer, H., and Chan, L. (2010). Glucose-6-phosphate mediates activation of the carbohydrate responsive binding protein (ChREBP). Biochem. Biophys. Res. Commun. *395*, 395–400.

Lin, J.H., Walter, P., and Yen, T.S. (2008). Endoplasmic reticulum stress in disease pathogenesis. Annu. Rev. Pathol. *3*, 399–425.

Liu, J.Z., Jellbauer, S., Poe, A.J., Ton, V., Pesciaroli, M., Kehl-Fie, T.E., Restrepo, N.A., Hosking, M.P., Edwards, R.A., Battistoni, A., et al. (2012). Zinc sequestration by the neutrophil protein calprotectin enhances Salmonella growth in the inflamed gut. Cell Host Microbe *11*, 227–239.

Liu, L., Lu, Y., Martinez, J., Bi, Y., Lian, G., Wang, T., Milasta, S., Wang, J., Yang, M., Liu, G., et al. (2016). Proinflammatory signal suppresses proliferation and shifts macrophage metabolism from Myc-dependent to HIF1α-dependent. Proc. Natl. Acad. Sci. USA *113*, 1564–1569.

Lund, J.M., Alexopoulou, L., Sato, A., Karow, M., Adams, N.C., Gale, N.W., Iwasaki, A., and Flavell, R.A. (2004). Recognition of single-stranded RNA viruses by Toll-like receptor 7. Proc. Natl. Acad. Sci. USA *101*, 5598–5603.

Ma, Y., Hof, P.R., Grant, S.C., Blackband, S.J., Bennett, R., Slatest, L., McGuigan, M.D., and Benveniste, H. (2005). A three-dimensional digital atlas database of the adult C57BL/6J mouse brain by magnetic resonance microscopy. Neuroscience *135*, 1203–1215.

Medzhitov, R., Schneider, D.S., and Soares, M.P. (2012). Disease tolerance as a defense strategy. Science *335*, 936–941.

Miller, N.E. (1964). Some psychophysiological studies of motivation and of the behavioural effects of illness. Bull. Br. Psychol. Soc. *17*, 1–20.

Miller, E.S., Bates, R.A., Koebel, D.A., Fuchs, B.B., and Sonnenfeld, G. (1998). 2-deoxy-D-glucose-induced metabolic stress enhances resistance to Listeria monocytogenes infection in mice. Physiol. Behav. *65*, 535–543.

Murray, M.J., and Murray, A.B. (1979). Anorexia of infection as a mechanism of host defense. Am. J. Clin. Nutr. *32*, 593–596.

Nairz, M., Ferring-Appel, D., Casarrubea, D., Sonnweber, T., Viatte, L., Schroll, A., Haschka, D., Fang, F.C., Hentze, M.W., Weiss, G., and Galy, B. (2015). Iron regulatory proteins mediate host resistance to Salmonella infection. Cell Host Microbe *18*, 254–261.

Pecchi, E., Dallaporta, M., Jean, A., Thirion, S., and Troadec, J.D. (2009). Prostaglandins and sickness behavior: old story, new insights. Physiol. Behav. *97*, 279–292.

Potthoff, M.J., Inagaki, T., Satapati, S., Ding, X., He, T., Goetz, R., Mohammadi, M., Finck, B.N., Mangelsdorf, D.J., Kliewer, S.A., and Burgess, S.C. (2009). FGF21 induces PGC-1α and regulates carbohydrate and fatty acid metabolism during the adaptive starvation response. Proc. Natl. Acad. Sci. USA *106*, 10853–10858.

Råberg, L., Sim, D., and Read, A.F. (2007). Disentangling genetic variation for resistance and tolerance to infectious diseases in animals. Science *318*, 812–814.

Sayyah, M., Javad-Pour, M., and Ghazi-Khansari, M. (2003). The bacterial endotoxin lipopolysaccharide enhances seizure susceptibility in mice: involvement of proinflammatory factors: nitric oxide and prostaglandins. Neuroscience *122*, 1073–1080.

Schneider, D.S., and Ayres, J.S. (2008). Two ways to survive infection: what resistance and tolerance can teach us about treating infectious diseases. Nat. Rev. Immunol. *8*, 889–895.

Seron-Arbeloa, C., Zamora-Elson, M., Labarta-Monzon, L., and Mallor-Bonet, T. (2013). Enteral nutrition in critical care. J. Clin. Med. Res. *5*, 1–11.

Shimazu, T., Hirschey, M.D., Newman, J., He, W., Shirakawa, K., Le Moan, N., Grueter, C.A., Lim, H., Saunders, L.R., Stevens, R.D., et al. (2013). Suppression of oxidative stress by β-hydroxybutyrate, an endogenous histone deacetylase inhibitor. Science *339*, 211–214.

Singer, B.H., Newstead, M.W., Zeng, X., Cooke, C.L., Thompson, R.C., Singer, K., Ghantasala, R., Parent, J.M., Murphy, G.G., Iwashyna, T.J., and Standiford, T.J. (2016). Cecal ligation and puncture results in long-term central nervous system myeloid inflammation. PLoS ONE *11*, e0149136.

Smorodintsev, A.A., Aksenov, O.A., Konstantinova, I.K., Vil'ner, L.M., and Tinufanov, A.V. (1978). [Comparative study of the toxicity of poly G-poly C and poly I-poly C in different objects]. Vopr. Virusol., 201–206.

Soares, M.P., Gozzelino, R., and Weis, S. (2014). Tissue damage control in disease tolerance. Trends Immunol. *35*, 483–494.

Song, Y., Shen, J., Lin, Y., Shen, J., Wu, X., Yan, Y., Zhou, L., Zhang, H., Zhou, Y., Cao, M., and Liu, Y. (2014). Up-regulation of podoplanin involves in neuronal apoptosis in LPS-induced neuroinflammation. Cell. Mol. Neurobiol. *34*, 839–849.

Tabas, I., and Ron, D. (2011). Integrating the mechanisms of apoptosis induced by endoplasmic reticulum stress. Nat. Cell Biol. *13*, 184–190.

Taubenberger, J.K., and Morens, D.M. (2008). The pathology of influenza virus infections. Annu. Rev. Pathol. *3*, 499–522.

Terbach, N., and Williams, R.S. (2009). Structure-function studies for the panacea, valproic acid. Biochem. Soc. Trans. *37*, 1126–1132.

van den Berghe, G., Wouters, P., Weekers, F., Verwaest, C., Bruyninckx, F., Schetz, M., Vlasselaers, D., Ferdinande, P., Lauwers, P., and Bouillon, R. (2001). Intensive insulin therapy in critically ill patients. N. Engl. J. Med. *345*, 1359–1367.

Wing, E.J., and Young, J.B. (1980). Acute starvation protects mice against Listeria monocytogenes. Infect. Immun. *28*, 771–776.

Yang, L., Xie, M., Yang, M., Yu, Y., Zhu, S., Hou, W., Kang, R., Lotze, M.T., Billiar, T.R., Wang, H., et al. (2014). PKM2 regulates the Warburg effect and promotes HMGB1 release in sepsis. Nat. Commun. *5*, 4436.

Yoo, S.H., Abdelmegeed, M.A., and Song, B.J. (2013). Activation of PPARα by Wy-14643 ameliorates systemic lipopolysaccharide-induced acute lung injury. Biochem. Biophys. Res. Commun. *436*, 366–371.

## STAR★METHODS

### KEY RESOURCES TABLE

| REAGENT or RESOURCE | SOURCE | IDENTIFIER |
|---|---|---|
| Antibodies | | |
| Rabbit polyclonal anti-β Tubulin | Santa Cruz | Cat#sc-9104; RRID: AB_2241191 |
| Mouse monoclonal anti-GADD153 (clone B-3) | Santa Cruz | Cat#sc-7351; RRID: AB_627411 |
| Hamster monoclonal anti-TNF alpha (clone TN3-19.12) | eBioscience | Cat#14-7423; RRID: AB_468492 |
| Rat monoclonal anti-IL-6 (clone MP5-20F3) | eBioscience | Cat#14-7061; RRID: AB_468423 |
| Biotin-conjugated rabbit polyclonal anti-TNF alpha | eBioscience | Cat#13-7341; RRID: AB_466951 |
| Biotin-conjugated rat monoclonal anti-IL-6 (clone MP5-32C11) | BD | Cat#554402; RRID: AB_395368 |
| Anti-mouse CD4 FITC (clone GK1.5) | eBioscience | Cat#11-0041; RRID: AB_464893 |
| Anti-mouse CD4 BV421 (clone GK1.5) | BioLegend | Cat#100438; RRID: AB_11203718 |
| Anti-mouse CD11c FITC (clone N418) | eBioscience | Cat#11-0114; RRID: AB_464941 |
| Anti-mouse B220 PE (clone RA3-6B2) | eBioscience | Cat#12-0452; RRID: AB_465673 |
| Anti-mouse Ly6G PE-Cy7 (clone RB6-8C5) | eBioscience | Cat#25-5931; RRID: AB_469663 |
| Anti-mouse CD45 APC-eFluor 780 (clone 30-F11) | eBioscience | Cat#47-0451; RRID: AB_1548781 |
| Anti-mouse NK1.1 PE (clone PK136) | eBioscience | Cat#12-5941; RRID: AB_466051 |
| Anti-mouse CD11b BV421 (clone M1/70) | eBioscience | Cat#12-0112; RRID: AB_465548 |
| Anti-mouse TCR beta FITC (clone H57-597) | eBioscience | Cat#11-5961; RRID: AB_465324 |
| Anti-mouse Ly6C PE (clone AL-21) | BD | Cat#560592; RRID: AB_1727556 |
| Anti-mouse CD8a APC (clone 53-6.7) | eBioscience | Cat#17-0081; RRID: AB_469335 |
| Anti-mouse F4/80 PE-Cy5 (clone BM8) | BioLegend | Cat#123112; RRID: AB_893482 |
| Anti-mouse CD16/32 (clone 93) | eBioscience | Cat#16-0161; RRID: AB_468900 |
| Annexin V FITC | eBioscience | Cat#BMS500FI/300, RRID: AB_2575600 |
| Chemicals, Peptides, and Recombinant Proteins | | |
| 2-deoxy-D-glucose | Sigma-Aldrich | Cat#G8270; CAS: 154-17-6 |
| D-mannoheptulose | Cayman Chemical | Cat#16548; CAS: 3615-44-9 |
| Valproic acid | Sigma-Aldrich | Cat#P4543; CAS: 1069-66-5 |
| Levetiracetam | Sigma-Aldrich | Cat#L8668; CAS: 102767-28-2 |
| Mouse recombinant FGF21 | R&D Systems | Cat#8409-FG/CF; GenPept: Q9JJN1 |
| Lipopolysaccharide from *E. coli* strain 055:B5 | Sigma-Aldrich | Cat#L2880 |
| Poly(I:C) | Invivogen | Cat#tlrl-pic-5 |
| BHI broth | BD | Cat#241830 |
| Thapsigargin | Cayman Chemical | Cat#10522; CAS: 67526-95-8 |
| Mouse recombinant IFNα | R&D Systems | Cat#12100-1; GenPept: NP_996753 |
| Dihydroethidium | Thermo Fisher Scientific | Cat#D1306; CAS: 28718-90-3 |
| DAPI | Thermo Fisher Scientific | Cat#D1168; CAS: 38483-26-0 |
| Propidium iodide | eBioscience | Cat#BMS500FI/300 |
| N-PER Neuronal Protein Extraction Reagent | Thermo Fisher Scientific | Cat#87792 |
| RNA-Bee | Tel Test, Inc | Cat#CS-501B |
| SMART MMLV Reverse Transcriptase | Clontech | Cat#639524 |
| Low ROX PerfeCTa SYBR Green SuperMix | Quanta | Cat#95056 |
| Ethidium monoazide bromide | Biotium | Cat#40015 |
| Critical Commercial Assays | | |
| Mouse IFNα ELISA kit | eBioscience | Cat#BMS6027 |
| Mouse IL-1β ELISA kit | eBioscience | Cat#88-7013 |
| Mouse Cardiac Troponin-I ELISA kit | Life Diagnostics | Cat#CTNI-1-HSP |

(*Continued on next page*)

*Continued*

| REAGENT or RESOURCE | SOURCE | IDENTIFIER |
|---|---|---|
| Alanine Transaminase Activity Assay Kit | Cayman Chemical | Cat#700260 |
| Non-esterified Fatty Acid Assay Reagent | Wako Diagnostics | Cat#999-34691, Cat#995-34791, Cat#991-34891, Cat#993-35191 |
| β-hydroxybutyrate Assay Kit | Cayman Chemical | Cat#700190 |
| RNeasy Mini Kit | QIAGEN | Cat#74106 |
| i-STAT CG4+ Cartridge | Abaxis Global Diagnostics | Cat#600-9000 |
| Experimental Models: Organisms/Strains | | |
| Mouse: C57BL/6J | The Jackson Laboratory | Stock No. 000664 |
| Mouse: CHOP KO: B6.129S(Cg)-*Ddit3*$^{tm2.1Dron}$/J | The Jackson Laboratory | Stock No. 005530 |
| Mouse: PPARα KO: B6;129S4-*Ppara*$^{tm1Gonz}$/J | The Jackson Laboratory | Stock No. 008154 |
| Mouse: IFNaR KO: B6.129S2-*Ifnar1*$^{tm1Agt}$/Mmjax | The Jackson Laboratory | Stock No. 32045 |
| Mouse: FGF21 KO | David J. Mangelsdorf (Potthoff et al., 2009) | RRID: MGI_4354176 |
| *Listeria monocytogenes*: Strain 10403s | Daniel A. Portnoy (Auerbuch et al., 2004) | N/A |
| Influenza: Strain A/WSN/33 | Akiko Iwasaki (Lund et al., 2004) | N/A |
| *Legionella pneumophila*: serogroup 1 strain JR32 | Craig R. Roy (Archer and Roy, 2006) | N/A |
| Sequence-Based Reagents | | |
| Primers for qPCR, see Table S1 | This paper | N/A |
| Software and Algorithms | | |
| Inveon Research Workplace | Siemens Healthineers | N/A |
| IDL 8.0 | Exelis Visual Information Solutions | N/A |
| Other | | |
| Medical food (Abbott Promote) | Abbott | Cat#50774 |
| Ketogenic diet | Envigo | Cat#TD.96355.PWD |
| Standard mouse chow (Teklad Global 18% Protein Rodent Diets) | Envigo | Cat#2018S |
| Pulse oximeter | Starr Life Sciences Corp. | MouseOx Plus |
| Rectal probe thermometer | Physitemp | TH-5 Thermalert |
| Handheld blood analyzer | Abaxis Global Diagnostics | VetScan i-STAT 1 |
| Lysing Matrix D, 2 mL Tube | MP Biomedicals | Cat#116913500 |
| Plasma separator tubes | BD | Cat#365985 |

## CONTACT FOR REAGENT AND RESOURCE SHARING

Further information and requests for reagents may be directed to, and will be fulfilled by the corresponding author Ruslan Medzhitov (ruslan.medzhitov@yale.edu).

## EXPERIMENTAL MODEL AND SUBJECT DETAILS

### Mice

All animal experiments were performed in accordance with institutional regulations after protocol review and approval by Yale University's Institutional Animal Care and Use Committee. Male C57BL/6J mice (The Jackson Laboratory Stock No. 000664) between 7 and 10 weeks of age were used for all animal experiments in this study except where indicated. CHOP knockout mice are strain B6.129S(Cg)-*Ddit3*$^{tm2.1Dron}$/J purchased from Jackson Laboratory (Stock No. 005530). PPARα knockout mice are strain B6;129S4-*Ppara*$^{tm1Gonz}$/J purchased from Jackson Laboratory (Stock No. 008154). FGF21 knockout mice were a generous gift from Dr. David J. Mangelsdorf. IFNaR knockout mice (strain B6.129S2-*Ifnar1*$^{tm1Agt}$/Mmjax, Jackson Laboratory Stock No. 32045) were a generous gift from Dr. Akiko Iwasaki.

For infection of mice, *Listeria monocytogenes* strain 10403s was originally obtained from the laboratory of Dr. Daniel Portnoy. *L. monocytogenes* was grown to log phase in brain heart infusion (BHI) broth (BD), washed once with PBS, and resuspended in fresh BHI. Mice were injected retro-orbitally with $5x10^4$ colony forming units (CFU) of *L. monocytogenes* diluted in PBS. Influenza virus strain A/WSN/33 was originally obtained from the laboratory of Dr. Akiko Iwasaki and was propagated using Madin-Darby Canine

Kidney (MDCK) cells and titrated to determine concentration by plaque assay described below. For influenza infection, mice were anesthetized with a ketamine/xylazine mixture and indicated plaque forming units (PFU) of influenza in 30 μl PBS was administered intranasally dropwise. *Legionella pneumophila* (wild-type serogroup 1 strain JR32) was originally obtained from the laboratory of Dr. Craig Roy and was grown on charcoal-yeast extract agar (Sigma-Aldrich) plates for 2 days, then cultured overnight in *N*-(2-acetamido)-2-aminoethanesulfonic acid (ACES)-buffered yeast extract (AYE) broth (10 g/liter yeast extract, 10 g/liter ACES, 0.4 g/liter L-cysteine HCl-H2O, 0.135 g/liter ferric nitrate, all components from Sigma-Aldrich) and grown to an optical density at 600 nm of 1 in AYE broth. *L. pneumophila* culture was then diluted in PBS and $1x10^6$ CFU in 40 μl PBS was administered intranasally dropwise to mice anesthetized with ketamine/xylazine.

For the LPS endotoxemia, mice were injected intraperitoneally with the indicated dose of LPS derived from *Escherichia coli* 055:B5 (Sigma-Aldrich) diluted in 100 μl PBS. For the Poly(I:C) viral inflammation model, mice were injected retro-orbitally with 30 mg/kg of high molecular weight Poly(I:C) (InvivoGen) diluted in 100 μl of normal saline provided by the manufacturer.

For feeding experiments, enteral nutrition/supplementation consisted of Abbott Promote (25%, 23%, and 52% calories from protein, fat, and carbohydrates, respectively) which is an enteral nutrition commonly used in supportive care of critically ill patients with a nearly identical nutritional profile to laboratory Global 2018 Teklad chow (24%, 18%, and 58% calories from protein, fat, and carbohydrates, respectively). Mice were gavaged PBS control or the equivalent of one kilocalorie of the indicated substance (glucose, casein, olive oil, or Abbott Promote) twice a day starting 8 hr post-infection in infection models and 1 hr post-injection in sterile inflammatory models.

For intraperitoneal administration of D-(+)-glucose (Sigma-Aldrich G8270), D-mannoheptulose (DMH, Cayman Chemical), and 2-deoxy-D-glucose (2DG, Sigma-Aldrich), mice were injected intraperitoneally with glucose (20 mg in 100 μl water), DMH (1 mg in 100 μl water) or 2DG (5 mg in 100 μl water) twice a day starting 8 hr post-infection in infection models and 1 hr post-injection in sterile inflammatory models. Valproic acid and levetiracetam were administered intraperitoneally starting 6 hr post-injection at 125 mg/kg and 18 mg/kg in 100 μl PBS, respectively. FGF21 supplementation was done by retro-orbital injection of recombinant mouse FGF21 (R&D Systems) twice daily at 5 ng in 100 μl PBS per injection.

Blood oxygen saturation, breath rate, and heart rate were measured by pulse oximetry using the MouseOx Plus (Starr Life Sciences Corp.). Core body temperature was measured by rectal probe thermometry (Physitemp TH-5 Thermalert). Fasting was performed by placing mice over wire-bottomed cages with food removed from the hopper. The ketogenic diet was purchased from Envigo. Venous pH was measured using an iSTAT 1 Handheld Analyzer (Abaxis) and the CG4+ cartridges as per manufacturer's instruction.

### Cell Culture

To prepare bone marrow derived macrophages (BMDMs), C57BL/6J mice were euthanized by $CO_2$ asphyxiation and femurs and tibias were isolated. The bones were cleansed with ethanol then washed with RPMI 1640 (Corning 10-040-CV), and pulverized in a mortar. Resulting contents were filtered through a 70 μm nylon cell strainer. This pulverizing and filtering process was repeated two more times, after which the resulting contents were treated with ACK lysing buffer (Lonza) for 5 min, then washed with RPMI, contents were centrifuged and the pellet was resuspended in macrophage growth medium (RPMI 1640 supplemented with 10% FBS (GIBCO), 1% penicillin-streptomycin (GIBCO), 2 mM L-glutamine (GIBCO), 1 mM sodium pyruvate (GIBCO), 0.01 M HEPES (AmericanBio), and 30% L929-conditioned media as a source of CSF-1), and plated on petri dishes. Macrophage growth medium was supplemented on day 3. Cells were plated for use on day 6. For assaying the effect of 2DG on *L. monocytogenes* replication in macrophages, BMDMs were plated at a density of $5x10^5$ in 24-well tissue culture plates. BMDMs were infected with $5x10^5$ of *L. monocytogenes* in the presence or absence of 2DG (2.5 mg/ml). After 24 hr, both supernatant and cell lysate were harvested for quantification of bacterial load.

To prepare mouse embryonic fibroblasts (MEFs), pregnant C57BL/6J female mice were euthanized by $CO_2$ asphyxiation at 13.5 to 14.5 days post conception. Embryos were harvested and washed in PBS. After removal of the head and visceral organs, the remaining tissue was washed in PBS then minced in 0.05% Trypsin with EDTA (GIBCO). After a 30 min incubation at 37°C, the minced tissue is washed with DMEM (Sigma-Aldrich), centrifuged and cell pellet re-suspended in complete MEF media (DMEM supplemented with 10% FBS, 1% penicillin-streptomycin, 2 mM L-glutamine, 1 mM sodium pyruvate, and 0.01 M HEPES). After overnight incubation, cells were trypisinized and filtered through 70 μm cell strainer and plated in complete MEF media. For assaying the effect of glucose and 2DG on various cell stress and cytokine treatments, MEFs were plated at a density of $1x10^5$ cells per well in a 24 well plate. After overnight rest, cells were treated with the indicated chemicals or cytokines in the presence of additional glucose (final concentration 9 g/L), 15 mM 2DG, or vehicle control. Thapsigargin (Cayman Chemical) was administered at 1 μM. Poly(I:C) was given at 20 μg/mL. Recombinant mouse IFNα (R&D Systems) was used at 1000 U/ml.

## METHOD DETAILS

### Quantification of Bacterial and Viral Loads

*L. monocytogenes* CFU titers were determined by plating titrated amounts of liver and spleen homogenate on BHI plates. Briefly, liver and spleen were harvested at indicated times post-infection and weighed. Tissue homogenates were generated by pushing the tissue through a 70 μm cell strainer using the plunger of a 5 ml syringe. Titrated dilutions of tissue homogenate were generated in 1% Triton X-100 (Sigma-Aldrich), plated on BHI plates, and grown overnight at 37°C. For in vitro assays testing the effect of 2DG on

*L. monocytogenes* growth in macrophages, titrated amounts of culture supernatant and cell lysate were plated on BHI plates and grown overnight at 37°C. To test the effect of 2DG on growth of *L. monocytogenes* in BHI broth, 5 x$10^3$ *L. monocytogenes* was inoculated into 25 ml of BHI with or without 10 mg/ml of 2DG. Flasks were incubated overnight. Titrated volumes of *L. monocytogenes* containing BHI broth were plated the following day on BHI plates and incubated overnight for quantification.

To determine influenza virus strain A/WSN/33 titers in the lung, lung tissue was harvested at the indicated times post-infection, weighed, and disrupted by bead homogenization. For viral titers in the bronchoalveolar lavage (BAL) fluid, mice were euthanized and trachea exposed. BAL was performed via cannulation of the trachea and lungs were lavaged with 1 ml of PBS. Virus titer was determined by infection of MDCK cells with titrated amounts of lung homogenate and BAL followed by addition of an agar overlay for 48 hr. Cell monolayers were then stained with crystal violet and plaque numbers were determined.

### Plasma Cytokine, Metabolite, and Tissue Injury Marker Analysis

Whole blood was harvested from mice by retro-orbital bleeding and plasma was isolated using lithium heparin coated plasma separator tubes (BD). Plasma TNFα and IL-6 concentration were assayed by sandwich ELISA using capture antibodies (eBioscience), biotin-conjugated detection antibodies (eBioscience and BD, respectively), HRP-conjugated streptavidin (BD), and TMB substrate reagent (BD). Plasma IFNα and IL-1β concentrations were assayed using kits according to the manufacturer's protocols (eBioscience). Plasma Tropinin-I concentration (Life Diagnostics) and Alanine Aminotransferase (ALT) activity (Cayman Chemical) were assayed using kits according to manufacturers' protocols. Plasma creatinine was assayed using HPLC by The George M. O'Brien Kidney Center at Yale. Plasma non-esterified fatty acid concentration was measured using a kit according the manufacturer's protocols (Wako Diagnostics). Plasma β-hydroxybutyrate concentrations were measured using a kit according the manufacturer's protocols (Cayman Chemical).

### RNA Extraction and Quantification

For tissue RNA extraction, tissues were harvested into RNA Bee RNA isolation reagent (Tel Test) and disrupted by bead homogenization in Lysing Matrix D tubes using a FastPrep-24 5G homogenizer (MP Biomedicals). RNA was extracted using the RNeasy Kit according to manufacturer's protocol (QIAGEN). For RNA extraction from cultured cells, RNA was harvested using phenol-chloroform extraction according to manufacturer's protocol (Tel Test). cDNA synthesis was performed using MMLV reverse transcriptase (Clontech) with oligo(dT) primers. qRT-PCR reactions were performed on either a CFX96 Real-Time System or CFX384 Real-Time System (Bio-Rad) using PerfeCTa SYBR Green SuperMix (Quanta Biosciences) and transcript levels were normalized to Rpl13a. Primers used for qRT-PCR are cataloged in Table S1.

### Flow Cytometry

Antibodies used for flow cytometry are cataloged in the antibodies section of the Key Resources Table. Cell viability was determined using ethidium monoazide bromide (EMA) following manufacturer's suggested protocol (Biotium). Samples were Fc-blocked with functional grade mouse anti-CD16/32 antibody (93) (eBioscience). Annexin V-FITC and PI were used for apoptosis assays following the manufacturer's protocol (eBioscience). For tissue analyses, at least 1 × $10^5$ cells were acquired on $CD45^+$ cells within the singlet live gate, as defined by size, granularity, and pulse-width. Samples were acquired on an LSRII flow cytometer (BD), and analyzed using FlowJo (Tree Star Technologies).

### In Vivo Reactive Oxygen Species Staining

24 hr after administration of indicated treatments, mice were injected with 0.2 mg of dihydroethidium in 100 μl PBS. After 30 min, mice were anesthetized with a ketamine/xylazine mixture and perfused with 4% paraformaldehyde. Brains were harvested and 50 micron sections were cut on a vibratome (Lancer Vibratome 1000 Plus). Sections were then stained with DAPI (ThermoFisher Scientific) for 48 hr and visualized immediately.

### Positron-Emission Tomography and Analyses

Mice were imaged on the Inveon small animal PET/CT scanner (Siemens Medical Solutions) using 5.3 ± 3.9 MBq of $^{18}$F-FDG. Mice were injected with either LPS or Poly(I:C), and two hours after challenge, injected with $^{18}$F-FDG. Mice were scanned for $^{18}$F-FDG localization continuously over two hours under isoflurane anesthesia. To draw the lung, heart, liver, and whole body ROIs, we used the Inveon Research Workplace (IRW) software (Siemens Healthineers). Regions-of-interest were manually drawn for the heart, liver, and lung, and we used a template for the brain (Ma et al., 2005). To co-register the brain images with the template of brain regions, J.G. manually estimated translations and rotations, using a custom-built visualization tool written in IDL 8.0 (Exelis Visual Information Solutions). Standard uptake values (SUVs) at 40-60 min post-injection were used to assess glucose metabolism.

### Histopathlogy

All mice were euthanized by carbon dioxide asphyxiation and perfused with PBS or fixative. Tissues were immersion-fixed in either 10% neutral buffered formalin or Bouin's fixative (Ricca Chemical Corporation). Tissues were trimmed, processed, embedded, and sectioned and stained for hematoxylin and eosin by routine methods. Tissues were evaluated by a veterinarian (C.J.B.) trained in veterinary pathology with extensive expertise in mouse pathology blinded to both experimental and genetic manipulations.

Digital light microscopic images were acquired using a Zeiss Axio Imager A1 microscope, an AxioCam MRc5 Camera, and AxioVision 4.8.3.0 imaging software (Carl Zeiss MicroImaging, Inc.). The resulting images were optimized using Adobe Photoshop 13.0.1x 64.

TUNEL staining was performed by the Yale Research Histology Service and the sections evaluated and photographed blind to experimental manipulation. For TUNEL staining quantification, at least 7 non-overlapping 400x magnification fields per mouse brain were counted for total nuclei and TUNEL-stained nuclei to generate a final % TUNEL-positive count. Counts were performed by three independent, blinded investigators and averaged.

### Western Blot

Hindbrain samples were harvested and snap frozen in liquid nitrogen. Frozen tissues were pulverized in liquid nitrogen, then protein extracted with N-PER Neuronal Protein Extraction Reagent (ThermoFisher Scientific), supplemented with HALT protease and phosphatase inhibitor cocktail (ThermoFisher Scientific), according to the manufacturer's protocols. Equal amounts of protein were loaded per well of a 10% Bis-Tris mini-gel (Invitrogen) and run in 1x MOPS buffer (Invitrogen). Protein was transferred onto activated PVDF membrane (Millipore), then blocked in 5% milk in TBST (20 mM Tris, 150 mM NaCl, 0.05% Tween 20) for 30 min. Membranes were incubated with primary antibodies mouse anti-GADD153 (B-3) and rabbit anti-β Tubulin (H-235), both from Santa Cruz, overnight at 4°C. Anti-GADD153 was incubated at 1:1000 dilution in SignalBoost reagent (Millipore). Anti-β Tubulin was incubated at 1:5000 dilution in 4% BSA TBST. Membranes were washed 3x with TBST, then incubated with secondary antibodies at 1:10,000 dilution for one hour at room temperature. After washing, protein was visualized using enhanced chemiluminescence reagent (ThermoFisher Scientific).

## QUANTIFICATION AND STATISTICAL ANALYSIS

Statistical information including n, mean, and statistical significance values are indicated in the text or the figure legends. Results were statistically analyzed using Student's t test or an analysis of variance (ANOVA) test with multiple comparisons where appropriate using Prism 6.0 (GraphPad Software, Inc). Kaplan Meier survival curves were compared using log-rank Mantel-Cox test. A p value of $< 0.05$ was considered to be statistically significant.

Cell

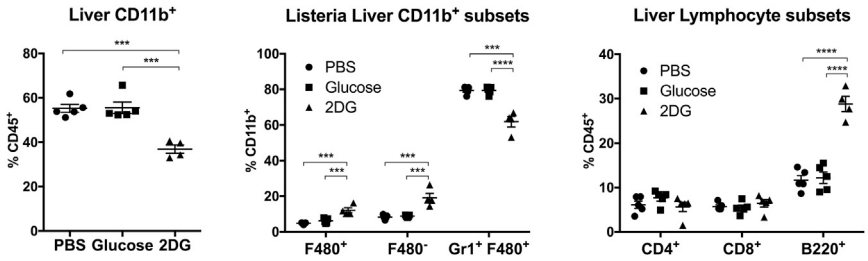


**Figure S1. The Effect of Glucose Caloric Supplementation or Inhibition of Glucose Utilization on Hepatic Immune Cell Infiltration during *L. monocytogenes* Infection, Related to Figure 1**

Flow cytometry analysis of $CD45^+$ cells within the liver 4 days after *L. monocytogenes* infection and treatment with PBS, glucose, or 2DG.
Data are represented as mean ± SEM. ***$p < 0.001$, ****$p < 0.0001$.

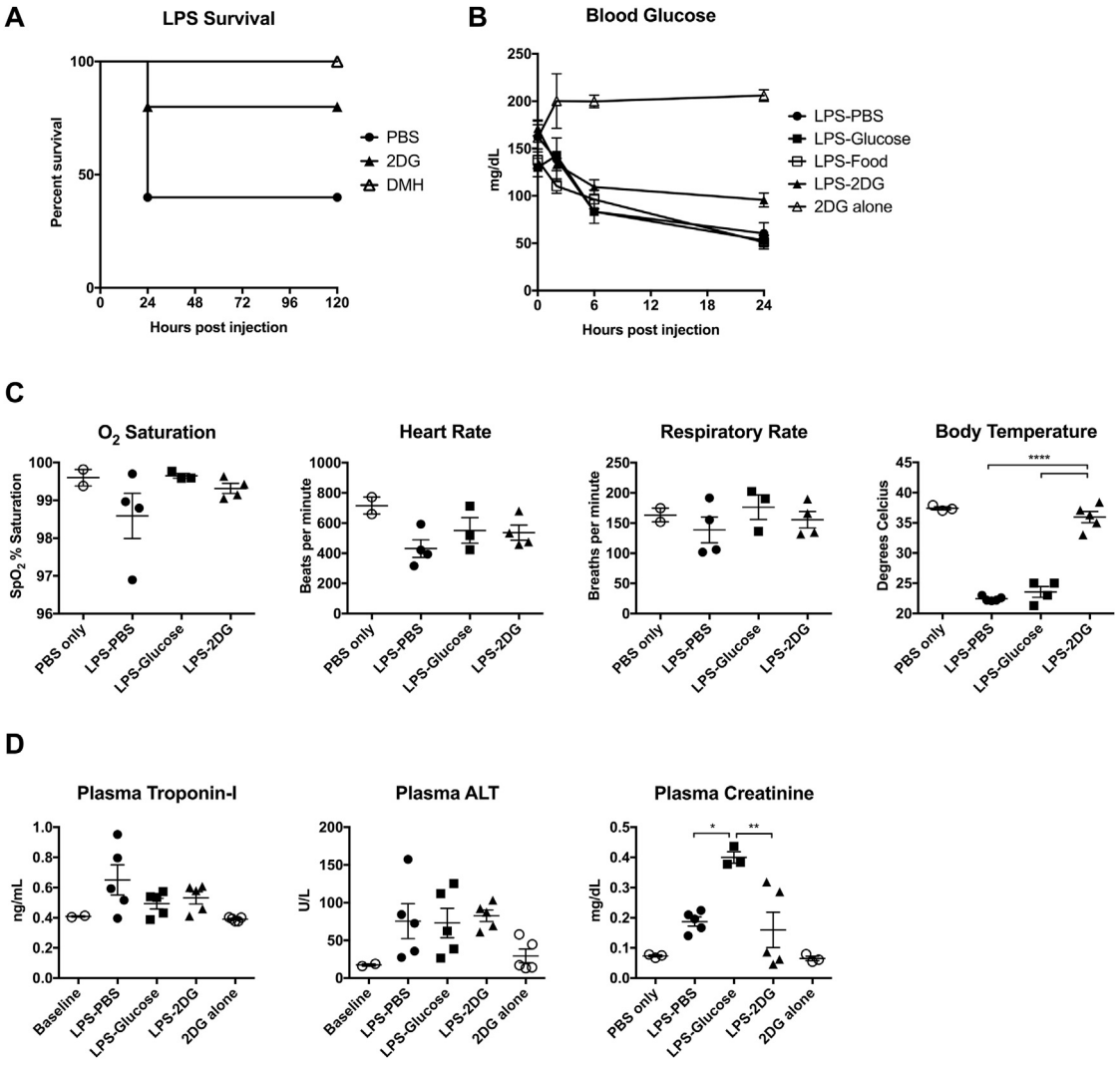


**Figure S2. Systemic Effects of Glucose Caloric Supplementation or Inhibition of Glucose Utilization during LPS Sepsis, Related to Figure 2**

(A) Mice were given 15 mg/kg IP LPS, then treated with PBS, 5 mg 2DG, 50 mg/kg D-mannoheptulose (DMH) given IP twice a day initiated one hour after LPS administration. n = 5/group.

(B) Blood glucose at baseline, 2, 6 and 24 hr after 15 mg/kg IP LPS with PO gavage of PBS vehicle (LPS-PBS), glucose (LPS-Glucose), or Abbott Promote (LPS-Food) BID; or with IP 2DG (LPS-2DG). Blood glucose of mice treated with only 2DG IP are also shown.

(C and D) Mice were given 15 mg/kg IP LPS, then treated with IP PBS, glucose, or 2DG given IP. (C) $O_2$ saturation, heart rate, respiratory rate, and body temperature 24 hr after LPS. (D) Plasma troponin-I, ALT, and creatinine levels measured at 24 hr after LPS.

Data are represented as mean ± SEM. *$p < 0.05$, **$p < 0.01$, ****$p < 0.0001$.

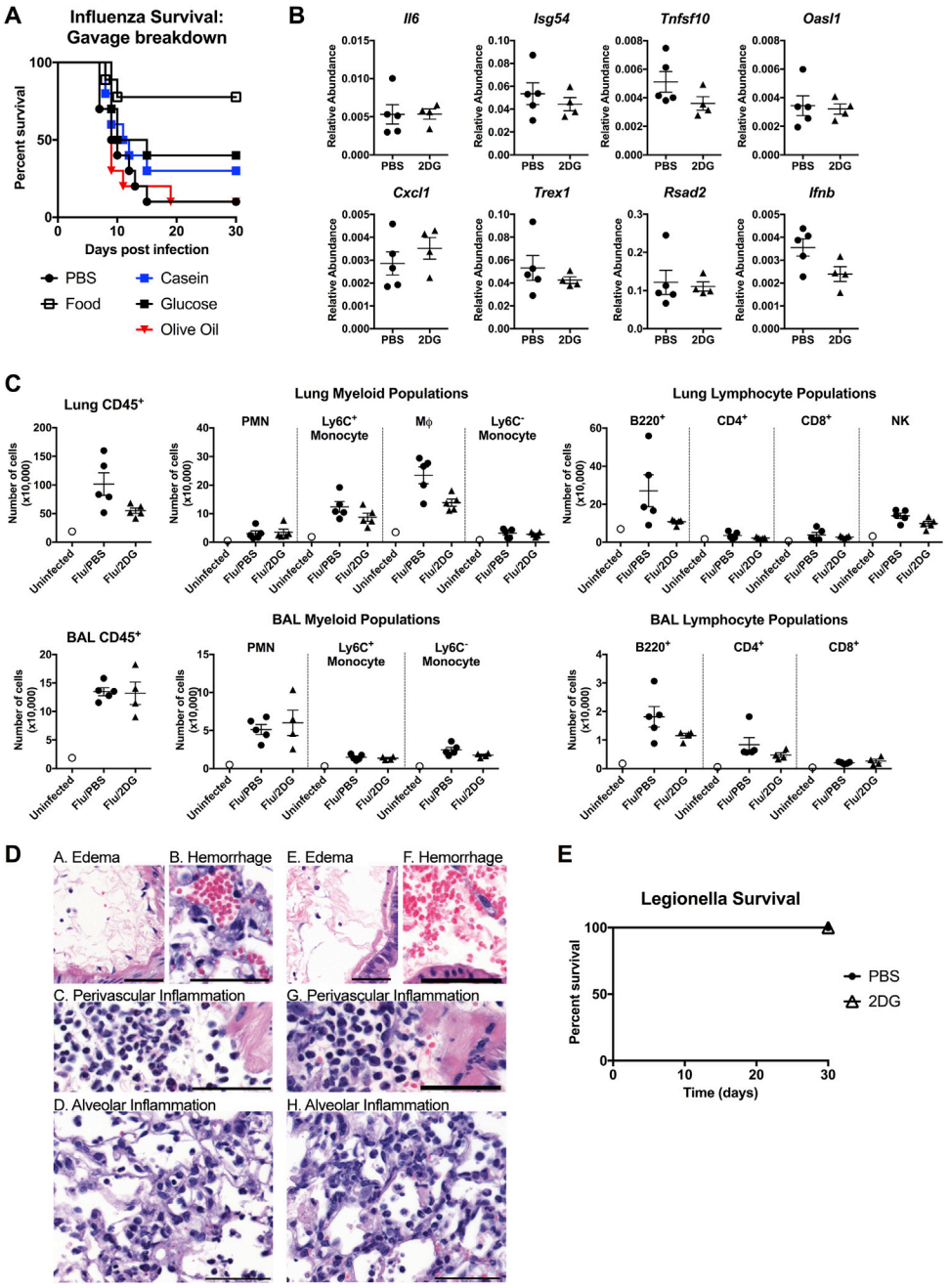


**Figure S3. The Effect of Caloric Supplementation or Inhibition of Glucose Utilization on Survival and Lung Inflammation after Influenza virus Infection, Related to Figure 3**

(A) Survival after infection with 800 PFU of influenza virus. Mice were gavaged with Abbott Promote (Food), casein, olive oil, or PBS vehicle. Figure 3B and 3C are a subset of Figure S3A, separated for clarity (the same PBS-treated and food-treated groups are shown).

(B) mRNA expression of whole lung tissue on day 6 after infection with 375 PFU of influenza virus and treatment with IP PBS or 2DG.

(C) Flow cytometric analysis of lung and BAL on day 6 after infection with 700 PFU of influenza virus and treatment with IP PBS or 2DG.

(D) H&E staining of lung tissue 6 days after infection with 375 PFU influenza virus and treatment with IP PBS or 2DG. Letters correspond to areas of the lung annotated in Figure 3. Scale bar = 50 μm.

(E) Survival after infection with $1x10^6$ *L. pneumophila*, and treatment with IP PBS or 2DG. n = 5/group.

Data are represented as mean ± SEM.

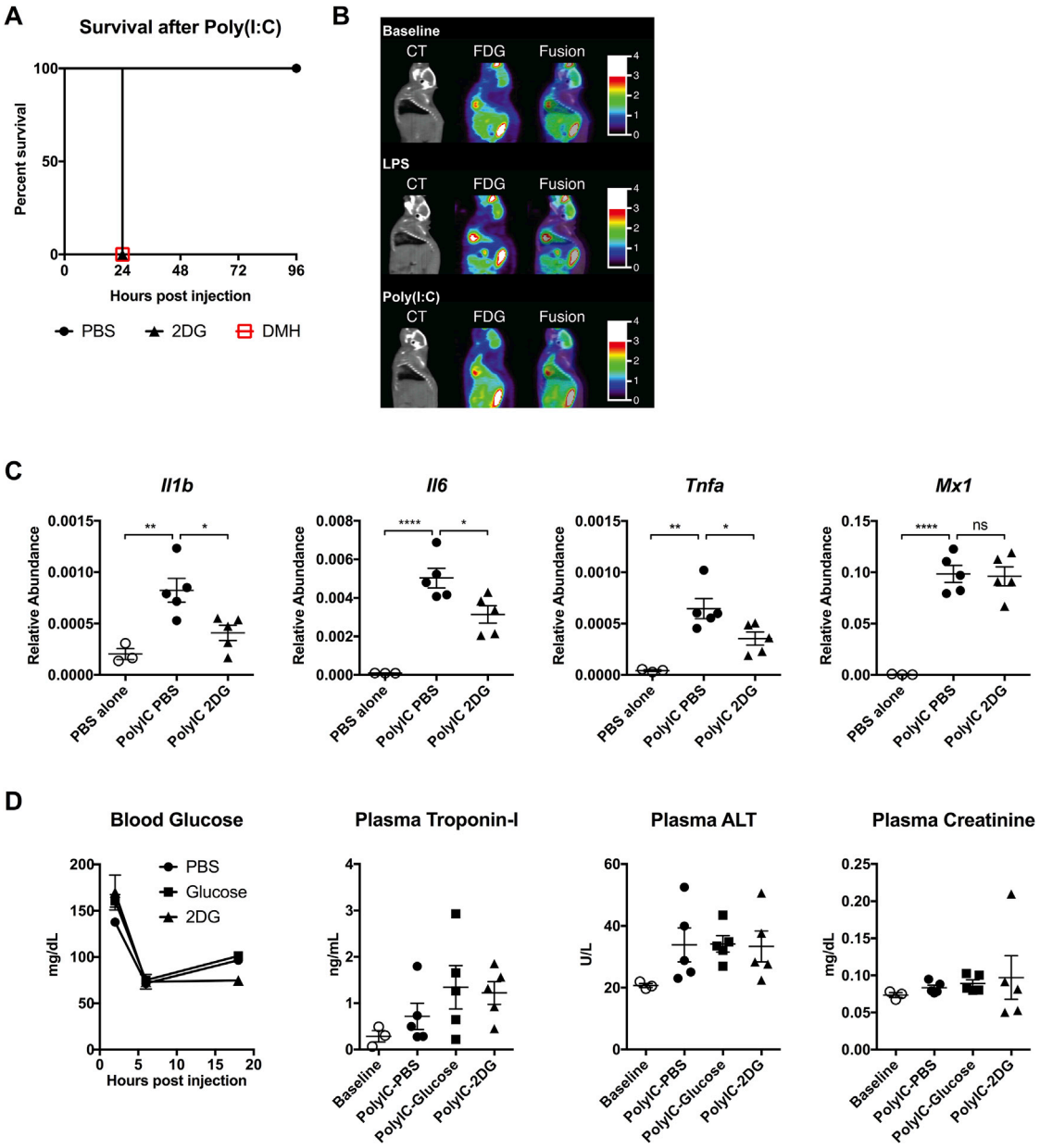


**Figure S4. Systemic Effects of Glucose Caloric Supplementation or Inhibition of Glucose Utilization during Poly(I:C) Sepsis, Related to Figure 4**

(A) Survival of mice after Poly(I:C) challenge and treatment with either IP PBS, 2DG, or DMH.

(B) Averaged sagittal PET images after PBS vehicle (baseline), LPS, and Poly(I:C) administration. CT, computed tomography; FDG, 2-deoxy-2-[$^{18}$F] fluorodeoxy-D-glucose. n = 3/group.

(C and D) Mice were challenged with Poly(I:C), then treated with either IP PBS, glucose, or 2DG. (C) Hindbrain mRNA expression 4 hr after Poly(I:C) administration and indicated treatments. n = 3-5/group. (D) Blood glucose measured at 2, 6, and 18 hr after Poly(I:C) and indicated treatments. Plasma troponin-I, ALT and creatinine measured at 24 hr after Poly(I:C).

Data are represented as mean ± SEM. *p < 0.05,**p < 0.01, ****p < 0.0001. n.s., not significant.

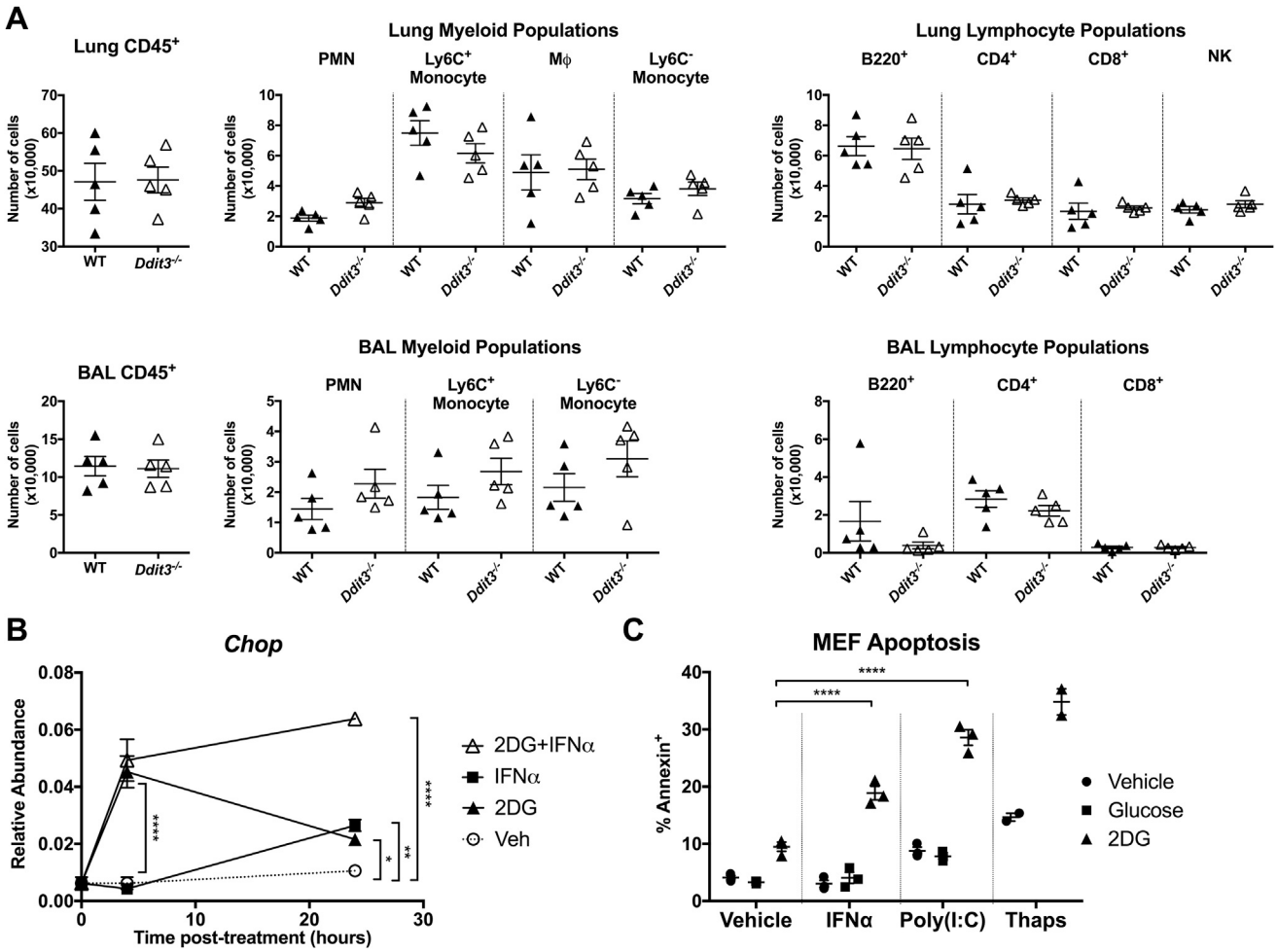


**Figure S5. The Effect of Inhibiting Glucose Utilization on Inflammation and ER Stress during Viral Inflammation, Related to Figure 5**

(A) Flow cytometric analysis of Lung and BAL on day 5 after infection with 700 PFU of influenza virus in B6 WT and *Ddit3*$^{-/-}$ mice.

(B) Mouse embryonic fibroblasts (MEFs) treated with vehicle, IFNα, 2DG, or IFNα and 2DG. mRNA expression at 0, 4, and 24 hr after treatment. n = 3 replicates per group. Data representative of two independent experiments.

(C) MEFs treated with vehicle, IFNα, Poly(I:C), and Thapsigargin (Thaps), in the presence of vehicle, glucose or 2DG for 24 hr. Flow cytometric analysis for Annexin V. Two-three replicates per group. Data representative of three independent experiments.

Data are represented as mean ± SEM. *p < 0.05,**p < 0.01, ****p < 0.0001.

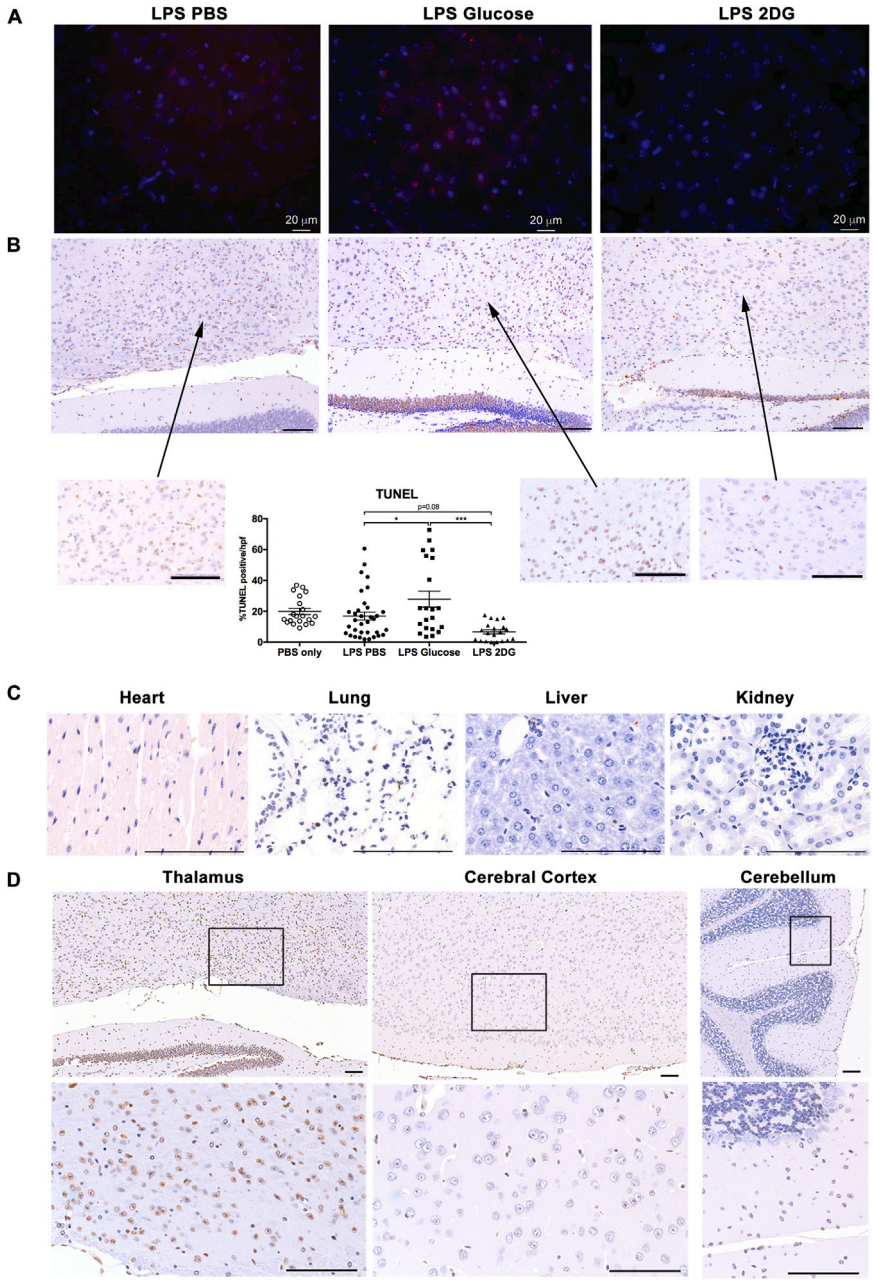


**Figure S6. Histopathology of LPS Sepsis, Related to Figure 6**

(A) Mice were given IP LPS then initiated with IP PBS, glucose, and 2DG treatment. Dihydroethidium staining of brain 24 hours after LPS.

(B) TUNEL-stained sections of brain 24 hours after LPS and treatment with PBS, glucose, or 2DG. 3,3'-Diaminobenzidine (DAB) hematoxylin, scale bars = 100 μm. Quantification of TUNEL positive cells per 400x power field. n=3/group.

(C) Representative images of TUNEL-stained sections of heart, lung, liver, and kidney 24 hours post-LPS. DAB Hematoxylin, scale bars = 100 μm.

(D) Representative sections of TUNEL-stained thalamus, cerebral cortex, and cerebellum 24 hours post-LPS in WT mice. DAB Hematoxylin, scale bars = 100 μm. Data are represented as mean ± SEM.

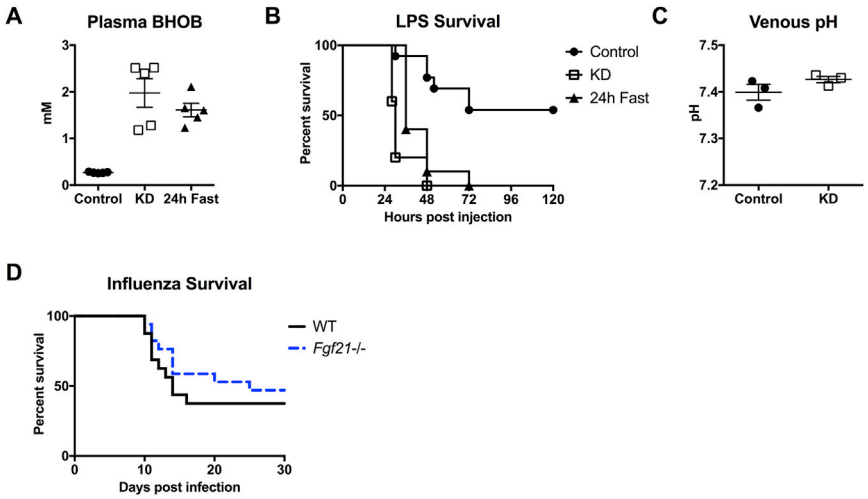


**Figure S7. Investigation of the Ketogenic Program in Bacterial and Viral Inflammation, Related to Figure 6**

(A) Plasma BHOB levels after 3 days of ketogenic diet (KD) and 24 hr of fasting compared to control fed mice. Control versus KD diet p = 0.0001; Control versus 24h Fast p = 0.0011. n = 5/group.

(B) Survival after 10 mg/kg IP LPS in mice on control diet, after 3 days of ketogenic diet (KD), and after 24 hr of fasting. Control versus KD p = 0.0002; Control versus 24h Fast p = 0.0007.

(C) Venous blood gas measured in mice on control diet and 3 days after ketogenic diet (KD).

(D) Survival after 375 PFU influenza in WT and *Fgf21*$^{-/-}$ mice.

Data are represented as mean ± SEM.